Observers, Blankets, and Screens

Executable Correspondences, Obstructions, and Complementarities across Observer Patch Holography, the Free Energy Principle, and Fuller's Synergetics

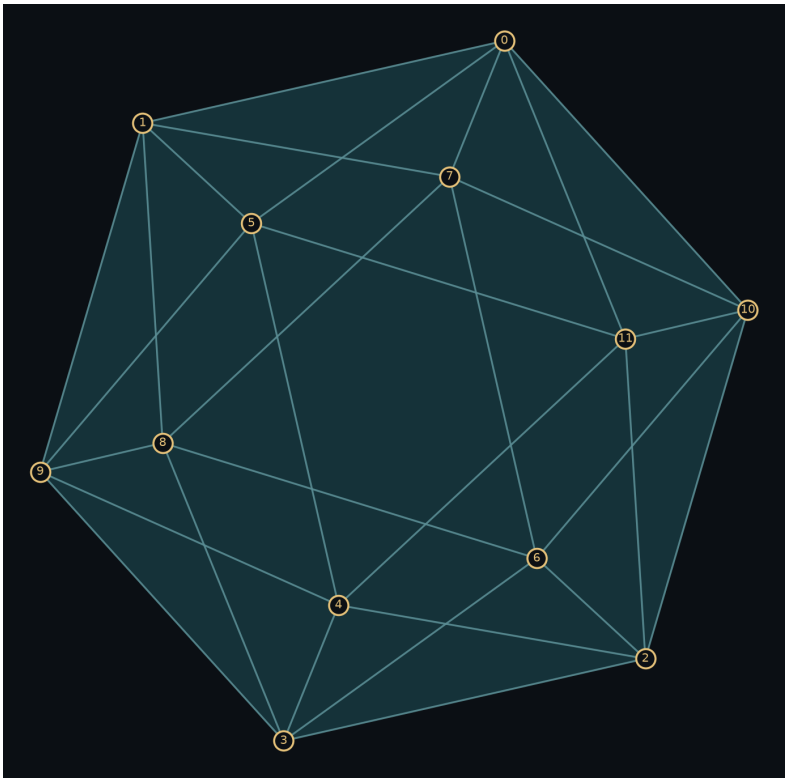
Daniel Ari Friedman

Active Inference Institute

daniel@activeinference.institute

ORCID: 0000-0001-6232-9096

November 15, 2026



1 Graphical abstract: three pairwise ledgers in four panels

Every claim in this paper is one **correspondence**: a statement about a single object, put in two or three vocabularies at once, executed by a probe that returns values rather than a verdict. The registry holds 44 such claims: 19 identifications, 15 obstructions and 10 complementarities, scoped to the pairs `oph-fep` (26), `synergetics-oph` (14), `fep-synergetics` (2) and `three-way` (2).

The four panels are the paper in pictures, one page each: the ledger of the three pairwise scopes; the carrier every scope is about; the dynamics that separates the readings; and the accounting, where the programmes disagree about currencies rather than facts.

1.1 Panel 1 — the pairwise ledger: what each pair of programmes agrees on, obstructs, and supplies

Each edge carries one pair's ledger in the form the command line executes it: `oph-fep-synergetics verify --pair oph-fep`, `--pair synergetics-oph`, `--pair fep-synergetics`. The centre carries the one claim that needs all three vocabularies at once. Most OPH–FEP work is obstruction: 26 claims, most of them failures of an identification proposed in good faith. Most Synergetics–OPH work is identification: 14 claims about symmetry, volume and counting. The FEP–Synergetics edge is short by 2 claims and holds two exact results about information, in one of which the programmes disagree about the meaning of a number.

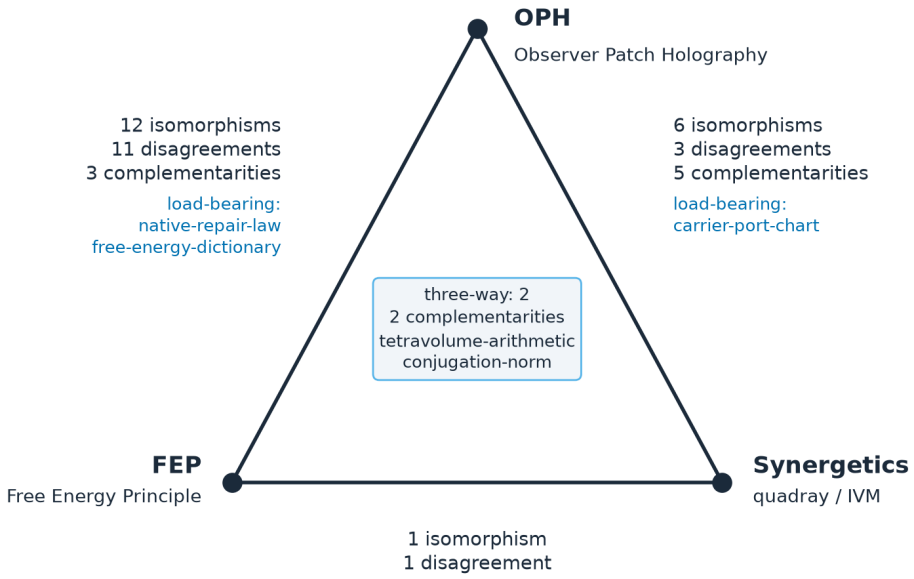
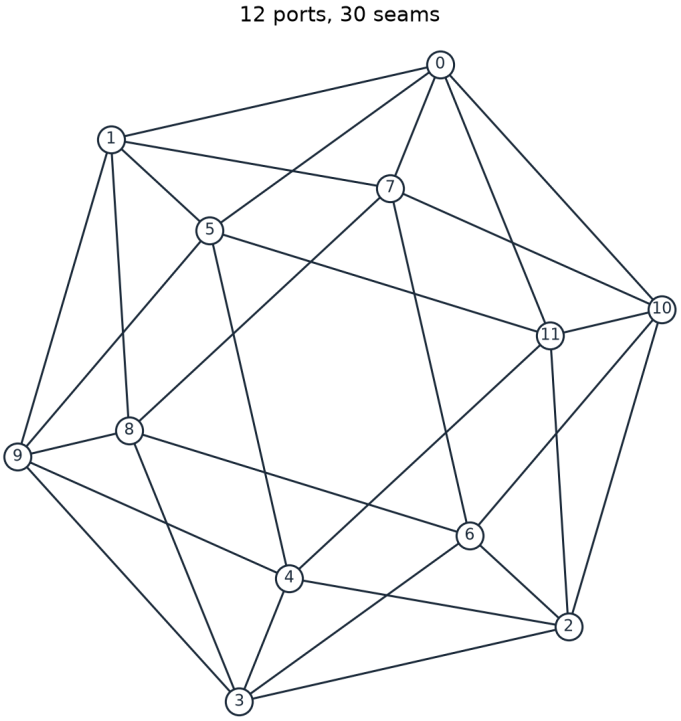


Figure 1: The pairwise ledger triangle. Vertices are the three programmes, Observer Patch Holography, the Free Energy Principle and Fuller's Synergetics. Each edge is annotated with the counts of identifications, obstructions and complementarities for that pair, and the three load-bearing identifications are named on the edge where they sit. The centre carries the three-way ledger: the two claims that need all three vocabularies at once, `tetravolume-arithmetic` – three exact quantities in three number systems – and `conjugation-norm`. Every count is read from the executed registry at draw time rather than transcribed.

The scope of a claim is part of the claim: `carrier-port-chart` is a statement about OPH's chart and the icosahedron's vertex set, `spectral-gap` is a statement about one matrix read two ways — the generator of OPH's mean repair operator and the FEP's precision — with the gap inherited from the shared object, and `kl-lattice-metric` is a statement about the FEP's divergence and Synergetics' lattice metric. sec. 6 reports the three ledgers separately, and tbl. 4 carries the scope of every row.

1.2 Panel 2 — the carrier: one graph, its symmetry, its counting identities, and its Gaussian reading

Every scope is read on the same object, so the paper can compare vocabularies without first having to reconcile subjects: twelve ports, thirty seams, twenty triangular faces, every port of degree 5, spectral gap 2.763932. OPH supplies the repair law on the seams of that graph. The FEP reads a diagonal shift of the Laplacian as a proper Gaussian precision. Two ports in this model are dependent given the rest exactly when they share a seam. The panel also carries two counting identities that neither programme states but both inherit from the graph: the number of spanning trees, and the dimensions of the agreement sheaf (Proposition 7; Proposition 9).



OPH-facing

spanning trees	5,184,000
dim H^0	1
dim H^1	19
symmetry group order	120
rotations	60
reflections	60

FEP-facing

intrinsic variance $(L^+)_{ii}$	7/36
proper Gaussian blanket size	5
pairwise precision	−1
on pairs	60

Figure 2: The carrier and its exact invariants. Left: the ports and seams drawn from their derived adjacency. Right: the spanning-tree count, sheaf dimensions, and symmetry counts, followed by centered intrinsic port variance and the proper Gaussian's blanket size and pairwise precision.

The reduced Laplacian of the seam graph has determinant 5184000, so the carrier has exactly that many spanning trees, and the same number is recovered from the spectrum as a product of eigenvalues. The scalar sheaf on the seam graph has a 1-dimensional space of global sections and 19 independent obstructions, the coboundary has rank 11, and the graph's Euler characteristic is -18, the twelve nodes minus the thirty edges; with the twenty faces added their boundaries span the cycle space, and the surface's Euler characteristic is 2. The carrier's automorphism group has order 120, splits into 60 rotations and 60 reflections when the orientation of OPH's own faces is used as the test, and acts on the 78 total-two configurations in 4 orbits with 3 distinct descent-outcome multisets. The proper Gaussian has seam precision -1 and a blanket of 5 neighbours per port. The centred intrinsic field gives port variance 0.1944444, exactly 7/36.

1.3 Panel 3 — native repair and Gaussian costs on lattice shells

Native repair takes a configuration, a seam and a coin. Of the 78 states in its census, 66 are binary. Over 4680 attempts, 120 lower the load energy, 600 move with the energy unchanged, and 3960 leave the state unchanged. The preceding panel's equivariance explains why this census is invariant under carrier symmetry. The separate lattice example compares equal-covariance Gaussian divergence with the IVM shell index.

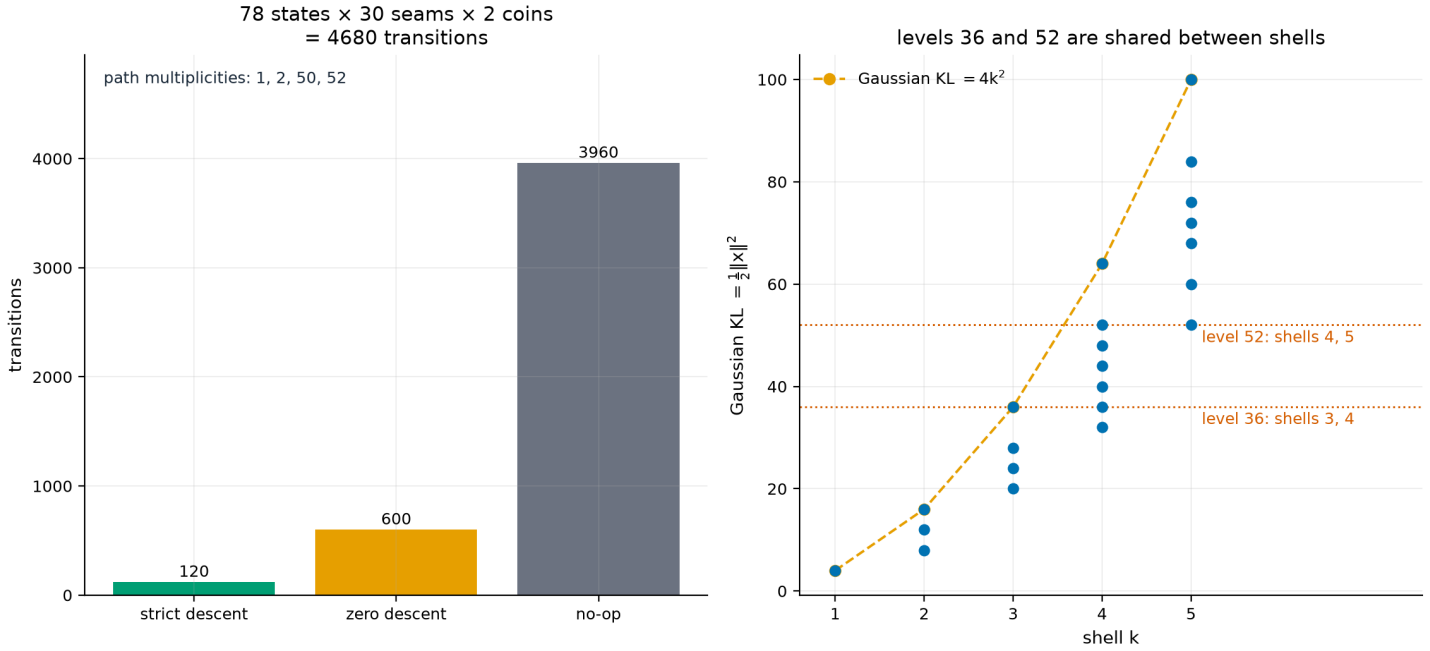


Figure 3: The descent census and the Gaussian divergence levels. Left: strict descents, zero descents and no-ops on the native load shell, with the path multiplicities. Right: half the squared norm over the first five IVM coordination shells, one column per shell, with shared levels marked.

One lattice step costs 4 nats at unit covariance, because the Gaussian divergence between equal-covariance neighbours is half the squared norm and the first shell sits at squared distance 8, so the sites at squared norm $8k^2$ cost $4k^2$. The first five shells carry (1, 3, 4, 7, 7) distinct free-energy levels, and the levels (36, 52) are each carried by two shells: the shell index does not fix the free energy, and the free energy does not fix the shell. The shell is a level set of a polyhedral norm and the free energy of a Euclidean one, and the obstruction is that neither refines the other.

1.4 Panel 4 — the accounting: tetravolumes, one packing, and three number systems

Synergetics counts volume in tetrahedra of the prime vector and asks which solids come out integral. The IVM's own solids do: (1, 3, 4, 6, 20, 96). The carrier's own solid does not: it enters at 18.5123 tetravolumes, which is $(5/2)(3\sqrt{2}+\sqrt{10})$ exactly. The same accounting settles the twelve-around-one question completely, because the cell of the twelve neighbours is a rhombic dodecahedron whose volume can be derived rather than looked up, and the ball inscribed in it gives the densest packing density in three dimensions [Hales, 2005].

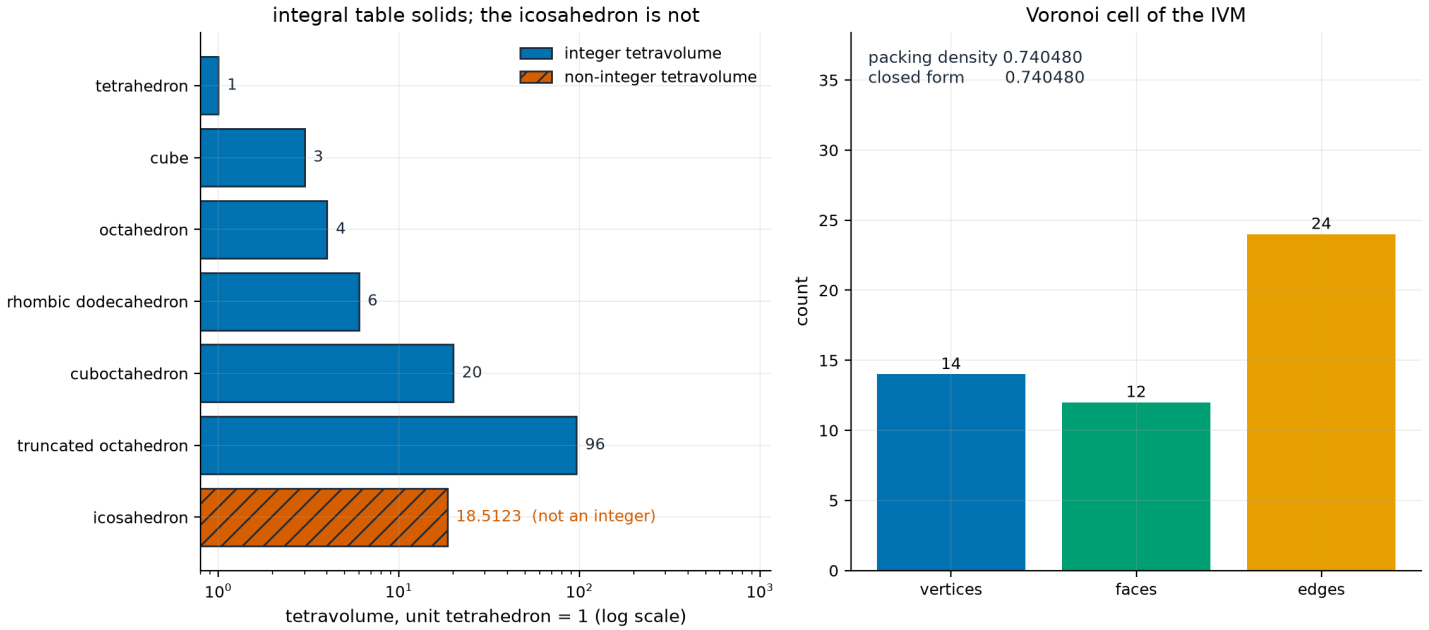


Figure 4: Tetravolume accounting and the twelve-around-one cell. Left: the tetravolumes of the IVM's integral solids beside the regular icosahedron's measured tetravolume on a logarithmic axis, showing that the carrier's own solid is the one entry an integer table cannot express. Right: the Voronoi cell of the twelve neighbours with its vertex, face and edge counts, its derived tetravolume from half the squared norm at each of its vertices, and the packing density of the inscribed ball against the closed form.

The cell of the twelve neighbours has 14 vertices, 12 faces and 24 edges, tetravolume 6 derived from the halved squared norm at each of its vertices, and an inscribed ball of 4.442883 tetravolumes which fills density 0.7404805, exactly $\pi\sqrt{2}/6 = \pi/(3\sqrt{2})$ because the cell's volume is rational and the ball's tetravolume is $\pi\sqrt{2}$. The carrier's icosahedron enters at 18.5123, computed exactly as $\sqrt{2}$ times an element of $\mathbb{Q}(\sqrt{5})$, with squared value 342.7051, exactly $175+75\sqrt{5}$, and is not integral: the tetravolume table and the carrier's own solid live in different arithmetics even though they are the same geometry. The three programmes' exact quantities live in three number systems: an integer 4 nats for the FEP's step, the quadratic surd 0.04606553 for OPH's relaxation rate, and integral tetravolumes beside one biquadratic one in Synergetics'.

Contents

1 Graphical abstract: three pairwise ledgers in four panels **2**
- 1.1 Panel 1 — the pairwise ledger: what each pair of programmes agrees on, obstructs, and supplies . . . 2
- 1.2 Panel 2 — the carrier: one graph, its symmetry, its counting identities, and its Gaussian reading . . . 3
- 1.3 Panel 3 — native repair and Gaussian costs on lattice shells . . . 4
- 1.4 Panel 4 — the accounting: tetravolumes, one packing, and three number systems . . . 5

2 Abstract: three programmes, one carrier, and a registry that executes every claim **8**

3 Introduction: three programmes of observer, one finite carrier, and a decision procedure for identification **9**
- 3.1 Three programs, one question . . . 9
- 3.2 What a correspondence is . . . 9
- 3.3 Contributions . . . 9
- 3.4 What this paper does not do . . . 10
- 3.5 Related work and positioning . . . 10

4 The three programs and the one object they share, stated in their own vocabularies **11**
- 4.1 The carrier . . . 11
- 4.2 OPH: a repair law on the seams . . . 11
- 4.3 FEP: a bound on surprisal . . . 12
- 4.4 Synergetics: tetravolume accounting . . . 13
- 4.5 One object, three vocabularies, and a dictionary this paper tests . . . 14

5 Method: a registry whose every claim is executed, scoped and re-runnable **15**
- 5.1 The unit of work . . . 15
- 5.2 The registry, grouped by pairwise scope . . . 15
- 5.3 Reading a source without copying it . . . 18
- 5.4 Why exactness, not agreement . . . 19

6 Agreement: the identifications each pairwise scope survives **20**
- 6.1 The port chart is a consequence, not a transcription . . . 20
- 6.2 The spectrum is closed-form . . . 20
- 6.3 The shell is counted exactly . . . 21
- 6.4 The native repair law is reproduced, not approximated . . . 21
- 6.5 Each native repair is exact conditioning . . . 22
- 6.6 The free-energy dictionary has a precise scope . . . 23
- 6.7 A sheaf computes the same Laplacian . . . 23
- 6.8 The carrier counts its own spanning trees . . . 24
- 6.9 The Gaussian reading makes the seam graph the independence graph . . . 24
- 6.10 Two cohomology dimensions, one global section . . . 24
- 6.11 The symmetry group closes the census . . . 25
- 6.12 Information cost is the synergetic metric over two . . . 25
- 6.13 The carrier's subgraphs are the solid's own counts . . . 26
- 6.14 Curvature is exact in units of pi . . . 26
- 6.15 What the agreements do not say . . . 26

7 Disagreement: the obstructions, each stated exactly **28**
- 7.1 The native law does not terminate . . . 28
- 7.2 Three distinct values at fixed records . . . 29
- 7.3 A stationary blanket does not bound the dynamics . . . 29
- 7.4 Stationary blankets leave entropy production free . . . 29
- 7.5 Stability is not generic in the coupling . . . 30
- 7.6 Reduction needs a threshold . . . 31
- 7.7 Existence does not imply reachability . . . 32
- 7.8 Direct and adjoint gradients differ . . . 32
- 7.9 The four-cycle has an incompatible local minimum . . . 33
- 7.10 Twelve vertices is not one solid . . . 33

7.11 The shell index and the free energy determine neither each other . . . 34
7.12 The shells around a port are not the lattice's shells . . . 34
7.13 `Twelve around one` names a family, not an object . . . 34
7.14 What the obstructions have in common . . . 36

8 Complementarity: structures one programme supplies and another needs 37
8.1 Synergetics supplies the accounting in which the carrier's geometry is exact . . . 37
8.2 The same quadratic sequence appears three times . . . 38
8.3 Energy-based learning supplies the gradient the repair law lacks . . . 38
8.4 Selection supplies a potential flow, for symmetric payoffs . . . 39
8.5 The carrier's own solid has an exact algebraic volume . . . 39
8.6 The densest packing in three dimensions has the twelve-around-one cell . . . 40
8.7 Three number systems and no common unit . . . 40
8.8 The precision also carries a resistance metric . . . 41
8.9 The twelve-around-one cell and the cuboctahedron are duals . . . 41
8.10 Conjugation fixes the counts and moves the volumes . . . 41
8.11 What the complements add up to . . . 41

9 Scope, limits and falsifiers of a correspondence battery 42
9.1 What is verified . . . 42
9.2 Three source quantities and their protocols . . . 43
9.3 What is not claimed . . . 43
9.4 Four cautions for anyone continuing this work . . . 43
9.5 What would change the conclusions . . . 43

10 Reproducibility: pins, commands, and the binding of every number to a function 45
10.1 What this manuscript is made of . . . 45
10.2 The three source pins . . . 45
10.3 The commands . . . 45
10.4 Environment . . . 46
10.5 What a reader should check first . . . 46

11 References 47

2 Abstract: three programmes, one carrier, and a registry that executes every claim

Three research programs describe observers in incompatible vocabularies. Observer Patch Holography builds spacetime from a finite complex of patches joined by seams, with a local repair law that moves load across those seams [FloatingPragma, 2026, Mueller et al., 2026]. The Free Energy Principle derives the behaviour of a self-maintaining system from a variational bound on surprisal [Friston, 2010, Parr et al., 2022]. Fuller's Synergetics axiomatises a closest-packed, tetravolume-counted geometry in which the twelve-around-one configuration is the unit of spatial accounting [Fuller and Applewhite, 1975, Edmondson, 1987].

This paper reports what happens when the three are made executable against one another. A registry of 44 correspondences was built, each one a claim scoped to a pair of programmes and carrying a probe that either reproduces an exact value or records the failure precisely: 19 isomorphisms, 15 disagreements and 10 complementarities. By scope, 26 claims relate OPH to the FEP, 14 relate Synergetics to OPH, 2 relate the FEP to Synergetics, and 2 entries need all three vocabularies at once. The load-bearing agreements are structural. OPH's carrier is a 12-port, 30-seam, 20-face complex whose adjacency is recovered from its own oriented faces, and its Laplacian spectrum is closed-form, with spectral gap `2.763932`. The native repair law conserves load and lowers a quadratic energy by a closed-form amount, and over the 78-configuration load shell it produces 120 strict descents, 600 zero descents and 3960 no-op moves out of 4680 transitions. On the binary shell each native repair is exact Bayesian conditioning on the datum it leaves visible, and its law minimises a variational free energy whose minimum is the surprisal of that datum [Mueller, 2026, Mueller et al., 2026].

Counting the same object turns out to add identifications that no dynamical reading supplies. The seam graph has 5184000 spanning trees, an integer that survives the surds in its own spectrum; the scalar sheaf on the seam graph has a 1-dimensional space of global sections (the constants) and 19 obstructions, the cycle rank. The face boundaries span the cycle space, giving surface Betti numbers (1, 0, 1). The automorphism group has order 120, splitting into 60 rotations and 60 reflections, transitive on ports, seams and faces, with the descent census invariant across all 78 configurations and 4 orbits under it. Its subgraphs are counted the same way: 20 triangles, exactly the faces the port chart was derived from, 12 five-cycles for the dual solid's vertices, 125 perfect matchings, and 1280 Hamiltonian cycles, with a curvature of 4 pi that is Gauss-Bonnet exactly and a resistance ladder whose exact fractions sum to a Kirchhoff index of 28. A proper Gaussian with diagonally shifted Laplacian precision has the seam graph as its conditional-dependence graph, with a Markov blanket of 5 neighbours per port. Separately, equal-covariance Gaussian divergence makes one lattice step cost 4 nats at unit covariance, half its squared distance in Synergetics' metric. Synergetics' accounting, every entry of which is derived here exactly from an explicit vertex set, then extends to the carrier's solid, which measures 18.5123 tetravolumes, an exact element of $\sqrt{2}\,\mathbb{Q}(\sqrt{5})$, against the integral table (1, 3, 4, 6, 20, 96), and to the twelve-around-one cell, whose 14 vertices, 12 faces and 24 edges give tetravolume 6 and the packing density 0.7404805, exactly $\pi/(3\sqrt{2})$.

The load-bearing disagreements are equally structural. On the tested shell the native law is confluent but does not terminate; the broken-seam gate terminates without giving unique normal forms. The binary-shell paths preserve load energy, while the ensemble can lose relative entropy. A pairwise reduction of a boundary exists only above a mediator threshold `0.3333333`; a blanket in the stationary density does not constrain the dynamics that preserve it; the solenoidal family leaves a stationary blanket's entropy production free [Mueller, 2026]; and four of the obstructions are failures of counting rather than of dynamics: twelve vertices do not determine a solid, a coordination shell and a free-energy level are not functions of one another, a neighbourhood is not a lattice shell, and the phrase "twelve around one" does not determine which solid is meant. Synergetics contributes the one geometry in which the other two can be drawn, not a derivation of either.

Three quantities the source literature states for the native law are reproduced exactly from OPH's public model, and the scope limits are stated rather than trimmed. Every number in this manuscript is bound to the function that produces it, every claim is executed by `oph-fep-synergetics verify` (or narrowed with `--pair` and `--kind`), and the graphical abstract on the preceding pages states the same results as four drawn panels.

3 Introduction: three programmes of observer, one finite carrier, and a decision procedure for identification

3.1 Three programs, one question

Observer Patch Holography (OPH) is a discrete reconstruction programme: a finite complex of patches carries integer load, seams between patches carry a repair law, and geometry is what the repair statistics look like from inside [FloatingPragma, 2026, Mueller et al., 2026, Friedman, 2026a]. The Free Energy Principle (FEP) is a variational programme: a system that persists must keep its sensory surprisal bounded, and the bound is a functional of a recognition density [Friston, 2010, 2013, Parr et al., 2022]. Synergetics is a geometric programme: spatial accounting is done in tetravolumes on a closest-packed lattice generated by twelve equal spheres around a central one, and the lattice's own sites and solids are counted with integers [Fuller and Applewhite, 1975, Friedman, 2025].

Each program answers a question the others only gesture at. OPH supplies a finite, exactly specified substrate and an explicit local update. FEP supplies the functional that a persisting system must be minimising, together with a statistical notion of a boundary. Synergetics supplies a coordinate system in which the lattice's finite configurations are counted without square roots, and this paper finds the one place where that fails: the carrier's own solid.

The question this paper asks is narrow enough to be answerable: *where the three programs make claims about the same finite object, do those claims agree?* Agreement here means more than analogy. Two claims agree when they can be stated as functions of the same object and the values coincide.

3.2 What a correspondence is

A correspondence is a record with four parts Definition 4: a claim, a pairwise scope, a probe, and a status. The claim names what OPH, FEP and Synergetics each say. The scope names which two or three of them the claim relates, because a claim that two vocabularies are about one object is a claim *about those two*. The probe is executable code that computes the values the claim rests on. The status is one of four terms, used in a fixed sense throughout sec. 5.

`exact` means the probe reproduces the claimed value exactly, in integers or rationals, or to floating-point equality with the closed form. `exact-on-domain` means the identification holds on a stated domain, typically the linear-Gaussian corner, and the probe asserts both the identity on that domain and its failure off it. `obstructed` means the identification fails, and the probe exhibits the failure with the same precision as a success. `not-reproduced` means the source asserts a quantity that its text does not determine, and the probe records the gap rather than inventing a value.

This vocabulary is the paper's main methodological commitment. An obstructed correspondence is a result, not a defect. It says where the three programmes cannot be welded together, and therefore where a synthesis has to choose.

3.3 Contributions

The contributions are the following.

1. A derived carrier. OPH's twelve-port adjacency is recovered from its twenty oriented faces rather than transcribed from a table, and the derivation is checked against an independent OPH consequence sec. 4.
2. A closed-form spectrum and gap for that carrier, the gap a quadratic surd and the multiplicities forced by the icosahedral group Proposition 2.
3. A complete census of the native repair law over the 78 configurations of total load two: 120 strict descents, 600 zero descents, 3960 no-op moves Proposition 14. The reachability probe separates the ungated law's nontermination from the gated law's lack of confluence Proposition 15.
4. An executable reproduction of Mueller's linear-Gaussian equivalence [Mueller, 2026, theorem 7, items 2–3]. The package checks the harmonic extension and the limit of predictive-coding perception against a separate KKT solve on the carrier Proposition 5.
5. Executable reproductions of Mueller's mediator, solenoidal and stability controls [Mueller, 2026, propositions 8–10 and 15]. The package derives the general Routh column and onset `3.162278` Proposition 18, verifies that the decomposition at the mediator threshold `0.3333333` uses rank-one blocks Proposition 19, and checks the solenoidal entropy production Proposition 17. Exact enumeration of the clipping regimes and an independent orbit measurement extend the two-node control Proposition 20.
6. An exact correspondence with Synergetics' IVM: twelve neighbour moves at squared distance 8, coordination shells of $10k^2 + 2$ sites identified in closed form as the lattice points on the frequency-k vector equilibrium, and the tetravolume table derived exactly from explicit vertex sets Proposition 4.

7. Two counting identities for the same carrier that no dynamical reading supplies: 5184000 spanning trees, and a sheaf whose 19 graph obstructions are exactly the face boundaries, so that the carrier's surface has Betti numbers (1, 0, 1) Proposition 8, Proposition 9.
8. The carrier's symmetry, which is what makes the census an invariant rather than a coincidence: order 120 split into 60 rotations and 60 reflections, irreducible eigenspaces, and a repair law equivariant transition by transition over 78 configurations in 4 orbits Proposition 10.
9. One place where the FEP's currency and Synergetics' metric are the same function: an equal-covariance divergence of 4 nats per lattice step at unit covariance, so a site at squared norm $8k^2$ costs $4k^2$ Proposition 11.
10. An exact volume for the carrier's own solid and for the twelve-around-one cell, both computed without floating point: 18.5123 tetravolumes, $\sqrt{2}$ times an element of $\mathbb{Q}(\sqrt{5})$ whose square is $175 + 75\sqrt{5}$, against an integral table, and a packing density of 0.7404805, exactly $\pi/(3\sqrt{2})$, derived from the cell rather than quoted Proposition 29, Proposition 30.
11. Five readings of the carrier as a network, none of which either programme supplied: exact effective resistances summing to a Kirchhoff index of 28, a subgraph census of 20 triangles, 12 five-cycles, 125 matchings and 1280 Hamiltonian cycles, and a curvature of 4 pi that is Gauss-Bonnet exactly Proposition 32, Proposition 12, Proposition 13.
12. A provenance discipline in which every source claim is pinned to a commit and every reimplementation cites the identifier it reimplements sec. 10.

Items 1 to 11 are executable: each is a function, and each section below reports the values that function returns.

3.4 What this paper does not do

It does not claim that OPH is a free energy principle, or that FEP is a holographic theory, or that Synergetics predicts either. It tests identifications from the integration proposals and runs the OPH–FEP controls developed in *Agreement and Surprise* [Friedman, 2026a,c, Mueller, 2026]. It reproduces the three quantities the source literature states for the native law from the protocols in OPH's public model sec. 9. It does not compare any of the three against laboratory data; OPH's own empirical status document is explicit that no retained comparison selects its record law, and this paper inherits that situation rather than resolving it [FloatingPragma, 2026].

3.5 Related work and positioning

The FEP literature contains its own internal disagreements, and this paper uses them as evidence rather than as noise. The Markov blanket is a statistical conditional-independence structure [Pearl, 1988], not automatically a dynamical object [Bruineberg et al., 2022], and technical objections to parts of the free energy principle have been stated precisely [Biehl et al., 2021]. The variational free energy is a bound, and its exactness conditions matter [Friston and Stephan, 2007, Sajid et al., 2021]. Bayesian mechanics gives the stationary-process reading of the same mathematics [Da Costa et al., 2021, Parr et al., 2020], and the discrete-state synthesis supplies the notation for the active-inference corner [Da Costa et al., 2020].

The title's third noun has a precedent on the FEP side: a Markov blanket has been read as a holographic screen, the boundary through which a system and its environment exchange information [Fields et al., 2022]. OPH's patches are screens in a different, discrete sense, and this paper does not identify the two; it records where their finite shadows agree. Bayesian mechanics has also been criticised from the physics side for how much of a system's dynamics a stationary blanket actually fixes [Aguilera et al., 2022], which is the question sec. 7.3 makes exact.

Synergetics has a small technical literature that states its conventions carefully [Edmondson, 1987], and the geodesic subdivision it motivates is the Goldberg construction [Goldberg, 1937] on the regular icosahedron [Coxeter, 1973], the same construction that classifies icosahedral virus shells [Caspar and Klug, 1962]. The lattice that results is the root lattice A3 in the closest-packing literature [Conway and Sloane, 1999], whose kissing number twelve was established by Schütte and van der Waerden [Schütte and van der Waerden, 1953] and whose coordination sequence is $10k^2 + 2$ [Conway and Sloane, 1997].

The tools this paper uses have long pedigrees, and it claims none of them: the algebraic connectivity of a graph [Fiedler, 1973], the Routh–Hurwitz criterion for a cubic [Routh, 1877, Hurwitz, 1895], Lyapunov stability [Khalil, 2002], contraction analysis [Lohmiller and Slotine, 1998], energy landscapes in neural networks [Hopfield, 1982], the information measures the surprises are built from [Shannon, 1948, Kullback and Leibler, 1951, Amari, 2016], topological signal processing [Ghrist, 2014], the Markov-blanket literature [Kirchhoff et al., 2018], and the predictive-processing reading of the free energy principle [Clark, 2013, Friston et al., 2017, Friston, 2019].

The contribution here is not a new theory but a decision procedure: a correspondence either executes or it does not, and the paper reports which.

4 The three programs and the one object they share, stated in their own vocabularies

4.1 The carrier

All three programs, read charitably, make claims about one finite object: a twelve-vertex, thirty-edge, twenty-face complex. This section fixes that object and then states each program's mathematics on it.

Definition 1. A **patch complex** is a finite simplicial complex $K = (V, E, F)$ with twelve vertices (*ports*), thirty edges (*seams*) and twenty triangular faces. A **load configuration** is a map $x \colon V \to \mathbb{Z}$; the *total load* is $\sum_v x_v$. A load configuration is **binary** when $x_v \in \{0, 1\}$ for every port. The **carrier** is the specific complex whose twenty oriented faces are those of the regular icosahedron under the port chart of [FloatingPragma, 2026].

The port chart is not decoration. OPH ships the twenty oriented faces, and the adjacency is a consequence of them: two ports are joined exactly when some face contains both. This package derives the adjacency that way and then asserts that the twenty triangles of the derived graph are exactly the twenty faces it started from, so a transcription error in either direction would be caught.

Proposition 1. The graph obtained from OPH's twenty oriented faces is 5-regular on 12 ports with 30 seams, and its 20 triangles are exactly the twenty generating faces.

The adjacency that results is listed in tbl. 1; it is reproduced here because the labelling differs from the common icosahedral labelling in which port 0 meets ports $1, 2, 3, 4, 6$, and a reader who assumes the common labelling will not reproduce any downstream number.

Table 1: The derived carrier adjacency: every port meets 5 others, and the triangles of this graph are exactly OPH's twenty oriented faces.

Port	Adjacent ports	Port	Adjacent ports
0	1, 5, 7, 10, 11	6	2, 3, 7, 8, 10
1	0, 5, 7, 8, 9	7	0, 1, 6, 8, 10
2	3, 4, 6, 10, 11	8	1, 3, 6, 7, 9
3	2, 4, 6, 8, 9	9	1, 3, 4, 5, 8
4	2, 3, 5, 9, 11	10	0, 2, 6, 7, 11
5	0, 1, 4, 9, 11	11	0, 2, 4, 5, 10

The carrier's Laplacian is the standard graph Laplacian $L = 5I - A$, which is how OPH writes it, and its spectrum is closed-form. The algebraic connectivity is $5 - \sqrt{5}$ [Fiedler, 1973], and the gap normalised by the total degree $2|E|$ is $(5 - \sqrt{5})/60$. In OPH's reading L is not the energy the repair law lowers (that is eq. 2 below); it is the generator of the *mean* repair operator $I - L/(2|E|)$ and the quadratic form of the seam-disagreement energy $\frac{1}{2}\sum_{\{a,b\}\in E}(x_a - x_b)^2 = \frac{1}{2}x^\top L x$.

Proposition 2. The carrier Laplacian has spectrum $\{0,\ (5-\sqrt{5})^{\times 3},\ 6^{\times 5},\ (5+\sqrt{5})^{\times 3}\}$, so $\lambda_1 = 5 - \sqrt{5} \approx 2.763932$ and $\lambda_1/(2|E|) = (5 - \sqrt{5})/60 = 0.04606553$.

The multiplicity pattern is the one forced by the icosahedral symmetry. The permutation representation of the full icosahedral group on the twelve ports splits into four pairwise inequivalent irreducibles, of dimensions one, three, five and three, so each eigenvalue's multiplicity is the dimension of one irreducible and no eigenspace contains two. The group fixes the eigenspaces and their dimensions; the four eigenvalues themselves are particular to $5I - A$ Proposition 10. fig. 5 draws the carrier and its spectrum.

4.2 OPH: a repair law on the seams

OPH's native dynamics is a local rule that moves integer load across a seam. On a seam joining ports a and b, with $d = x_a - x_b$ and a coin $c \in \{0, 1\}$, the amount moved is

$$\delta \;=\; \frac{d - (2c-1)\,(|d| \bmod 2)}{2}, \qquad x_a \leftarrow x_a - \delta, \quad x_b \leftarrow x_b + \delta. \tag{1}$$

The rule is written this way, rather than as "move half the difference", because it must stay in the integers: the parity correction is what keeps δ integral when d is odd. The quadratic energy

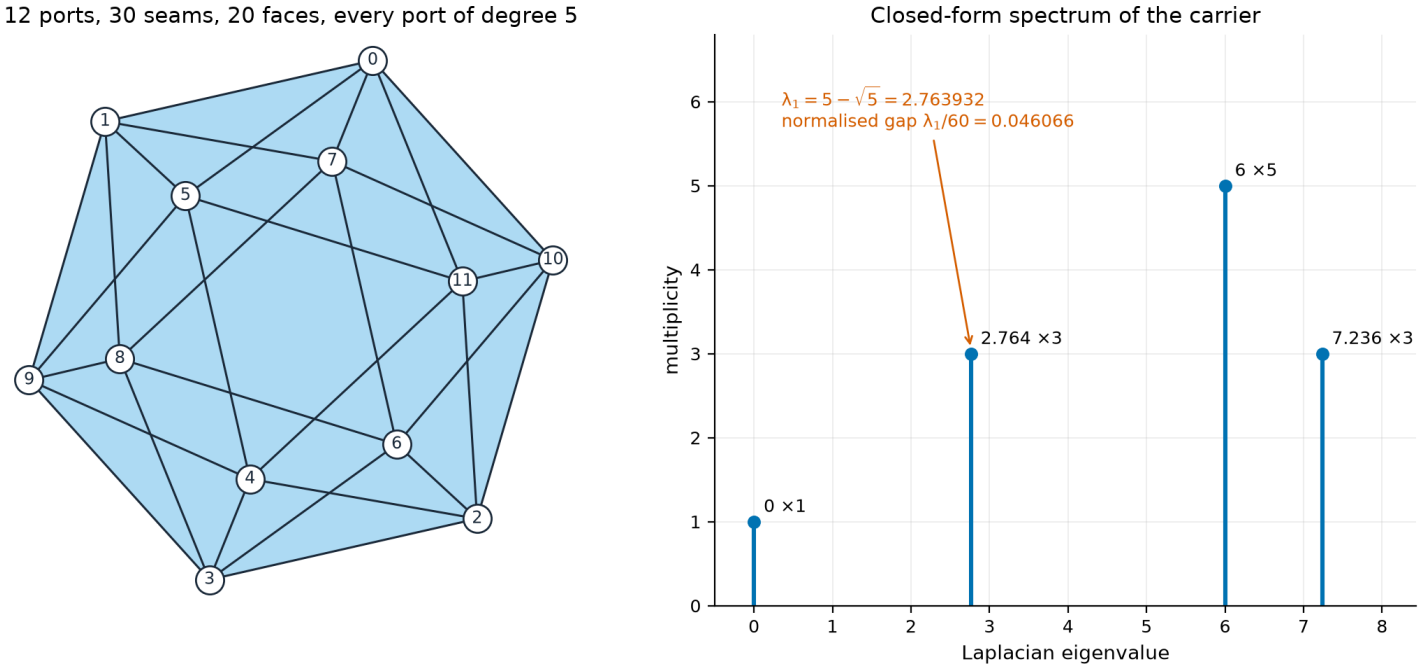


Figure 5: The carrier and its spectrum. Left: the twelve ports in their icosahedral positions, with the thirty seams drawn and the twenty faces shaded; ports are labelled with the chart of tbl. 1. Right: the Laplacian spectrum, with the zero eigenvalue, the three-dimensional eigenspace at $5-\sqrt{5}$, the five-dimensional eigenspace at six, the three-dimensional eigenspace at $5+\sqrt{5}$, and the normalised gap marked. Generated by `scripts/make_figures.py` from `core/carrier.py`.

$$E(x) \;=\; \tfrac{1}{2}\sum_{v\in V} x_v^2 \tag{2}$$

is the load energy. It never increases under the native repair.

Proposition 3. Under eq. 1 the total load is conserved and $\Delta E = -(d^2 - (|d| \bmod 2))/4$.

At $|d| = 1$ the decrease is exactly zero. The coin selects either a wait or a swap, and the swap changes the state at constant load energy. This is the pathwise obstruction tested in sec. 7.1.

Definition 2. The **load shell** of total q (OPH's shell, a level set of the total load; not to be confused with the lattice's coordination shells of Definition 3) is the set $\Sigma_q = \{x \in \mathbb{Z}^V_{\geq 0} : \sum_v x_v = q\}$. The shell of total two has $|\Sigma_2| = \binom{13}{11} = 78$ configurations, of which 66 are binary.

4.3 FEP: a bound on surprisal

The Free Energy Principle starts from a system with sensory states o and internal states s, and a recognition density $q(s)$. The variational free energy is

$$\mathcal{F}[q] \;=\; \mathbb{E}_q[-\log p(o,s)] \;-\; \mathbb{E}_q[-\log q(s)] \;=\; D_{\mathrm{KL}}[q(s)\,\|\,p(s\mid o)] \;-\; \log p(o), \tag{3}$$

so that minimising $\mathcal{F}$ over q at fixed o is minimising a divergence, and $-\mathcal{F}$ is a lower bound on the log evidence, the evidence lower bound [Friston, 2010, Friston and Stephan, 2007]. The bound is tight exactly when the recognition density is the posterior; the residual is the divergence.

In the linear-Gaussian construction, partition the carrier Laplacian L into recorded ports o and free ports x. The seam energy is $E(x,o) = \frac{1}{2}z^\top L z$, with $z = (x,o)$. At least one record grounds the interior block L_{xx}. A record prior $\rho(o) = \frac{1}{2}\epsilon\|o\|^2$ with $\epsilon > 0$ grounds the full precision. Integrating the resulting probability density over x gives the record surprisal [Mueller, 2026, theorem 7]:

$$-\ln p(o) \;=\; \tfrac{1}{2} o^{\top}(S+\epsilon I)o + \tfrac{d_o}{2}\ln(2\pi) - \tfrac{1}{2}\ln\det(S+\epsilon I), \tag{4}$$

where d_o is the number of record coordinates and S is the Schur complement of L_{xx} in L. The interior Gaussian determinant appears in the raw integral of $\exp(-E)$ and cancels in the probability density. With the prior fixed, eq. 4 gives an absolute value and determines the minimum of eq. 3 over q. The probes compare this marginal route to an energy-minus-entropy route that uses the full joint precision.

A **Markov blanket** is a partition of the state into interior i, blanket b and exterior e such that the interior and exterior are conditionally independent given the blanket:

$$p(i, e \mid b) \;=\; p(i \mid b)\, p(e \mid b). \tag{5}$$

eq. 5 is a statement about a probability distribution. It becomes a statement about dynamics only under further conditions, which is the content of Proposition 16.

4.4 Synergetics: tetravolume accounting

Synergetics replaces Cartesian coordinates with four signed counts whose sum is free, the **quadray** coordinates eq. 6. A quadray $q = (a, b, c, d)$ is an equivalence class,

$$(a, b, c, d) \;\sim\; (a+t,\, b+t,\, c+t,\, d+t) \qquad \text{for every } t \in \mathbb{R}, \tag{6}$$

so that a point is determined by differences. In the default embedding the four axes map to the vertices `(1, 1, 1)`, `(-1, 1, -1)`, `(-1, -1, 1)` and `(1, -1, -1)` of a regular tetrahedron, and in the integer lattice the twelve nearest neighbours of the origin are the distinct permutations of $(2, 1, 1, 0)$:

$$\mathcal{N} \;=\; \{\, \pi(2,1,1,0) \;:\; \pi \text{ a permutation} \,\}, \qquad |\mathcal{N}| = 12. \tag{7}$$

This is the twelve-around-one configuration, the *vector equilibrium* of Synergetics and the kissing configuration of the A3 root lattice, the face-centred cubic lattice [Conway and Sloane, 1999, Schütte and van der Waerden, 1953]. The neighbours are at squared distance 8 in the default embedding, so this embedding's unit of length is half the edge of the cube whose face diagonals are the neighbour moves; every Euclidean number below is stated in that unit.

Definition 3. The **coordination shell** S_k is the set of lattice sites at graph distance exactly k from the origin in the graph whose edges are the twelve neighbour moves. Halving the embedded coordinates maps the lattice onto $D_3 = \{u \in \mathbb{Z}^3 : u_1 + u_2 + u_3 \equiv 0 \pmod 2\}$, where the graph distance has the closed form

$$g(u) \;=\; \max(\|u\|_\infty,\; \tfrac{1}{2}\|u\|_1), \qquad |S_k| \;=\; 10k^2 + 2 \quad (k \geq 1). \tag{8}$$

g is the gauge function of the cuboctahedron whose vertices are the twelve neighbours, so S_k is the set of lattice points on the surface of the frequency-k vector equilibrium.

The count $10k^2 + 2$ is the coordination sequence of the face-centred cubic lattice [Conway and Sloane, 1997] and QuadMath's shell formula [Friedman, 2025]; the package builds the shells by breadth-first expansion and checks the closed form g against every site through shell 12. A coordination shell is a polyhedral surface, not a sphere: it meets several Euclidean spheres, which is the content of Proposition 22.

The tetravolume of a lattice simplex is the absolute determinant of its three edge vectors, each written in quadray coordinates with its fourth coordinate subtracted from the other three, divided by four, so the regular tetrahedron of the four axes has volume one. The six solids of Synergetics' table then have integer volumes, tetrahedron 1, cube 3, octahedron 4, rhombic dodecahedron 6, cuboctahedron 20, truncated octahedron 96, and the package derives every entry exactly from an explicit vertex set rather than reading it from the table (sec. 8.1). No square root appears in the accounting of the lattice's own solids, which is the point of the convention [Fuller and Applewhite, 1975, 1979, Edmondson, 1987]; the one solid that needs one is the carrier's (sec. 8.5).

Proposition 4. The quadray lattice generated by eq. 7 has 12 neighbour moves, all at squared distance 8, coordination shells of $10k^2 + 2$ sites with cumulative counts `(1, 13, 55, 147, 309)` for $k = 0, \ldots, 4$, and tetravolume ratios `tetrahedron`

`1, cube 3, octahedron 4, rhombic dodecahedron 6, cuboctahedron 20, truncated octahedron 96`, each derived exactly.

4.5 One object, three vocabularies, and a dictionary this paper tests

tbl. 2 states the translation the rest of the paper tests. It is a dictionary, not an argument: each row asserts that two terms denote the same mathematical object, and sec. 6 reports whether the assertion survives execution.

Table 2: The vocabulary dictionary this paper tests. Each row is a claim, and the last column names the registry entries whose probes execute it; sec. 6 reports the verdicts. The last two rows are the ones where the dictionary is least conservative, because a solid is not a graph: the agreements there are statements about the same geometry read from different constructions, and sec. 7.10 reports where reading them as the same solid fails.

OPH	FEP	Synergetics	probed by
port (patch)	coordinate of the generative model	quadray site	`carrier-port-chart`
seam	edge of the precision graph	IVM neighbour move	`gmrf-independence`, `kl-lattice-metric`
load configuration	state of the recognition density	site occupancy	`shell-counts`
seam repair	variational update	local re-accounting	`native-repair-law`, `variational-equivalence`
total load	conserved quantity of the dynamics	no counterpart: a load total is not a shell frequency	`native-repair-law`, `shell-counts`
{12, 30, 20} carrier	blanket-structured precision graph	icosahedron on the IVM	`carrier-port-chart`, `gmrf-independence`, `kissing-twelve`
carrier automorphisms	symmetries of the precision	icosahedral group of order 120	`icosahedral-symmetry`
obstructed seam cycles	frustrated cycle space of the precision	cycle rank 19 for the identity sheaf	`sheaf-cohomology`
one shell step	one divergence step of 4 nats	one move of squared distance 8	`kl-lattice-metric`, `tetravolume-arithmetic`
the carrier's twenty faces	faces of the simplicial complex	icosahedron of 18.5123 tetravolumes	`subgraph-census`, `icosahedron-tetravolume`
the twelve-around-one cell	neighbourhood of one coordinate	rhombic dodecahedron of 6 tetravolumes	`packing-density`, `dual-cells`

The dictionary is deliberately conservative. It does not say that a port *is* a quadray site, only that the two play the same role in the three formalisms and that the resulting numbers must therefore agree where both are defined. Where the numbers do not agree, sec. 7 says so. The carrier's counting invariants — 5184000 spanning trees, 19 sheaf obstructions, 120 automorphisms, and a census of 20 triangles, 12 five-cycles, 125 matchings and 1280 Hamiltonian cycles — are derived from the same complex in sec. 6, and each of them is a statement that two vocabularies inherit rather than assert.

5 Method: a registry whose every claim is executed, scoped and re-runnable

5.1 The unit of work

The paper's unit is a **correspondence**: a claim about the same object made in two or three vocabularies, together with executable evidence and an explicit pairwise scope.

Definition 4. A **correspondence** is a record $c = (\kappa, \rho, \sigma, \pi)$ where κ names the claim in the OPH, FEP and Synergetics vocabularies, ρ is the *pairwise scope*, one of `oph-fep`, `fep-synergetics`, `synergetics-oph` or `three-way`, naming the two or three programmes the claim relates, σ is a status from the fixed vocabulary below, and π is a *probe*: a total function from no arguments to a mapping from names to values. The probe **passes** when every value it reports satisfies the assertion the claim makes.

The scope ρ is not bookkeeping. A correspondence is a claim that two vocabularies are talking about one object, and which two they are is part of the claim: the same icosahedral symmetry is a statement about OPH and Synergetics, while the Markov blanket of the carrier precision is a statement about OPH and the FEP. sec. 6 reports the three pairwise ledgers separately for that reason, and `oph-fep-synergetics verify --pair synergetics-oph` executes one ledger on its own. The kind of a claim is selectable the same way: `oph-fep-synergetics verify --kind disagreement` runs the obstructions alone, so a reader who wants the failures does not have to read past the identifications.

Making the probe return values rather than a boolean is the single design choice that keeps the registry honest. A boolean can be made true by weakening a tolerance; a mapping of named values has to be *right*, and it can be compared against a source that states a different value.

Table 3: The status vocabulary. It is closed: a new status requires a new definition.

Status	Meaning
`exact`	the probe reproduces the claim exactly: integers, rationals, or closed-form surds
`exact-on-domain`	the identification holds on a stated domain and the probe asserts the boundary
`obstructed`	the identification fails, and the probe exhibits the failure precisely
`not-reproduced`	the source states a quantity its text does not determine; recorded, never invented

5.2 The registry, grouped by pairwise scope

tbl. 4 is the registry, reproduced from `src/oph_fep_synergetics/analysis/registry.py`. The grouping is the paper's argument in miniature: 19 claims survive as identifications, 15 fail as identifications while remaining informative, and 10 are complements in which one program supplies what another lacks without either reducing to the other. By scope, 26 claims relate OPH to the FEP, 14 relate Synergetics to OPH, 2 relate the FEP to Synergetics, and 2 entries need all three vocabularies at once.

Table 4: The 44 correspondences, in registry order: 19 isomorphisms, 15 disagreements and 10 complementarities, scoped `oph-fep` 26, `synergetics-oph` 14, `fep-synergetics` 2, `three-way` 2. Every row is executed by `oph-fep-synergetics verify`.

Key	Kind	Status	Pair	What it tests
`carrier-port-chart`	isomorphism	`exact`	`synergetics-oph`	derived adjacency reproduces the twenty oriented faces
`spectral-gap`	isomorphism	`exact`	`oph-fep`	one matrix read two ways (mean-repair generator and precision): $\lambda_1 = 5 - \sqrt{5}$, normalised gap $(5 - \sqrt{5})/60$
`shell-counts`	isomorphism	`exact`	`oph-fep`	the total-two load shell and its binary sub-shell, enumerated and checked against closed forms — the finite domain both oph-fep readings evaluate on

Key	Kind	Status	Pair	What it tests
native-repair-law	isomorphism	exact	oph-fep	OPH's integer rule reimplemented, with its closed-form energy drop
variational-equivalence	isomorphism	exact-on-domain	oph-fep	harmonic extension, constrained (KKT) minimiser and perception flow coincide; free energy at the posterior equals the surprisal
free-energy-dictionary	isomorphism	exact-on-domain	oph-fep	Gaussian carrier prior gives normalised surprisal, and the residual quadratic equals the KL between posteriors
sheaf-agreement	isomorphism	exact	oph-fep	the cellular sheaf Laplacian is the carrier Laplacian
certificate-species	isomorphism	exact	oph-fep	the certificate species of the shell and its spectral gap
tree-number	isomorphism	exact	oph-fep	one determinant, two readings: 5184000 counts spanning trees and normalises the FEP's Gaussian interface integral
gmrf-independence	isomorphism	exact	oph-fep	the seam graph is the conditional-independence graph of the precision: dependence exactly on the seams; blanket 5, variance 0.1944444
sheaf-cohomology	isomorphism	exact	oph-fep	patch agreement is the global-section condition: $\dim H^0 = 1$, $\dim H^1 = 19$ on the graph; with the faces, Betti numbers (1, 0, 1)
icosahedral-symmetry	isomorphism	exact	synergetics-oph	order 120, transitive on ports, seams and faces: 60 rotations, 60 reflections
eigenspace-irreducibility	isomorphism	exact	synergetics-oph	the eigenspaces are the group's non-trivial real irreducibles: dimensions (3, 3, 5) forced by the group and established by the commutant test
law-equivariance	isomorphism	exact	synergetics-oph	every transition commutes with every automorphism; 4 orbits, 3 outcome multisets
kl-lattice-metric	isomorphism	exact	fep-synergetics	one IVM step costs four nats and squared norm $8k^2$ costs $4k^2$
pr01-obstruction	disagreement	obstructed	oph-fep	ungated repair does not terminate; the gate can give different normal forms
free-energy-name-collision	disagreement	obstructed	oph-fep	"free energy" names inequivalent functionals
mediator-obstruction	disagreement	obstructed	oph-fep	pairwise boundary reduction needs a threshold
stationary-blanket	disagreement	obstructed	oph-fep	a stationary blanket is not an attractor
solenoidal-freedom	disagreement	obstructed	oph-fep	stationary blankets leave entropy production free
d-stability	disagreement	obstructed	oph-fep	stability is not generic in the coupling
schedule-path	disagreement	obstructed	oph-fep	iteration schedules are not interchangeable
reduction-criterion	disagreement	obstructed	oph-fep	competing reduction criteria disagree

Key	Kind	Status	Pair	What it tests
existence-without-reachability	disagreement	obstructed	oph-fep	existence of an equilibrium does not imply reachability
directed-gradient	disagreement	obstructed	oph-fep	direct and adjoint gradients differ
four-cycle-local-minimum	disagreement	obstructed	oph-fep	the four-cycle has spurious local minima
cuboctahedron-vs-icosahedron	disagreement	obstructed	synergetics-oph	twelve vertices is not one solid: tetravolume 20 against 18.5123 ...
shell-vs-free-energy	disagreement	obstructed	fep-synergetics	the coordination shell (a polyhedral norm) and the divergence (a Euclidean one) determine neither each other; levels (36, 52) are shared
quadray-ivm	complementarity	exact	synergetics-oph	IVM coordinates supply exact geometry; the tetravolume table is derived from vertex sets
equilibrium-propagation	complementarity	exact	oph-fep	the energy-based learning identity holds exactly
replicator-potential	complementarity	exact	oph-fep	the replicator field is a Shahshahani gradient for symmetric payoffs, and not otherwise
kissing-twelve	complementarity	exact	synergetics-oph	both twelve-around-one arrangements attain the kissing number: the cuboctahedral rigidly, the icosahedral with slack
icosahedron-tetravolume	complementarity	exact	synergetics-oph	the carrier's solid is 18.5123 ..., squared exactly $175 + 75\sqrt{5}$
packing-density	complementarity	exact	synergetics-oph	Voronoi cell 14/12/24, tetravolume six, density $\pi/(3\sqrt{2})$
tetravolume-arithmetic	complementarity	exact	three-way	integer nats, a surd gap, and an integral table beside a non-integral carrier
effective-resistance	complementarity	exact	oph-fep	effective resistance 11/30, 7/15, 1/2 by distance class, Kirchhoff index 28 twice over
two-record-resistance	isomorphism	exact	oph-fep	the inverse effective resistance sets the Schur energy of a pair's record contrast
vertex-shells	disagreement	obstructed	synergetics-oph	shells (5, 5, 1) against the lattice's (12, 42, 92); intersection array (5, 2, 1; 1, 2, 5)
subgraph-census	isomorphism	exact	synergetics-oph	20 triangles, 12 pentagons, 125 matchings, 1280 Hamiltonian cycles, counted by exhaustion
angle-defect	isomorphism	exact	synergetics-oph	OPH's derived chart is the icosahedron's triangulation, so the angular-defect accounting applies unchanged: $\pi/3$ at each port, 4π in total, which is $2\pi\chi$
twelve-around-one-families	disagreement	obstructed	synergetics-oph	the phrase covers solids with 5184000 and $331776 = 576^2$ spanning trees
dual-cells	complementarity	exact	synergetics-oph	the cell and the cuboctahedron, 14/12/24 against 12/14/24, volumes 6 and 20

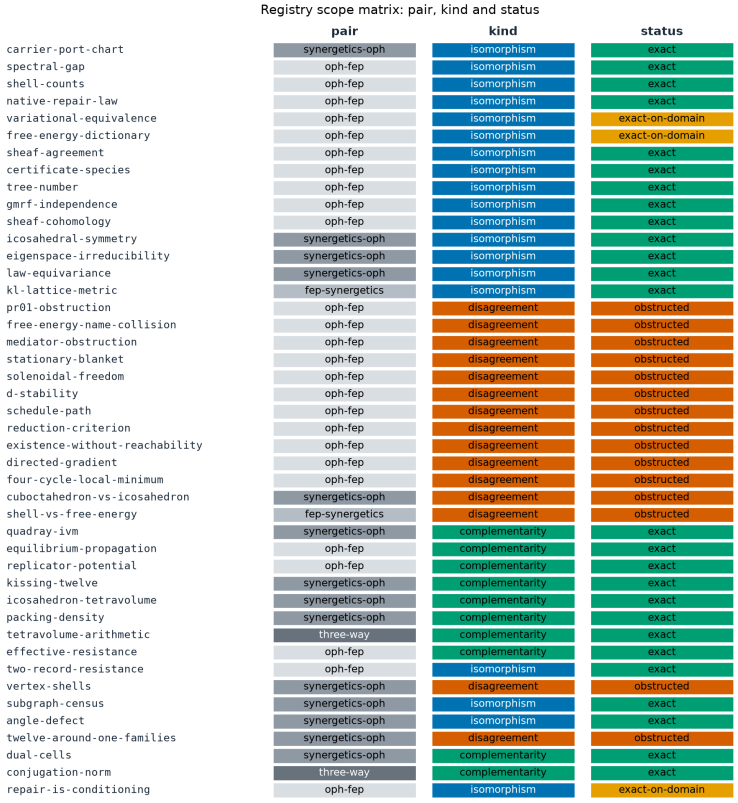


Figure 6: The registry as a scope matrix. Each row is one correspondence in registry order; the columns are its pairwise scope, its kind, its status, and whether the entry carries an executable probe, with cells coloured by category. The figure is drawn from `analysis/registry.py`, so an entry cannot appear in the matrix without appearing in `verify`.

Key	Kind	Status	Pair	What it tests
`conjugation-norm`	complementarity	`exact`	`three-way`	conjugation fixes the integer counts and moves the volume, whose norm is 50
`repair-is-conditioning`	isomorphism	`exact-on-domain`	`oph-fep`	on the binary shell each native repair is the uniform reference conditioned on its visible datum and minimises a free energy over the fibre; off the shell it fails on 60 seams

The registry is the source of truth for the paper. The prose in sec. 6, sec. 7 and sec. 8 says what the probes found; it does not add claims the probes do not carry. fig. 6 shows the same 44 rows as a matrix of scope, kind and status, so that the shape of the registry is visible without reading the table.

5.3 Reading a source without copying it

The three source programs are read at pinned commits, and the pins are data, not prose: `data/sources.json` records the commit, the branch, the licence terms and, for each borrowed identifier, the file, the line range and the symbol. The command `oph-fep-synergetics sources --vault-root <root>` re-reads the live checkouts and reports `match`, `moved`, `absent` or `unavailable` for each pin.

Three rules follow from the licences, and they are enforced rather than recommended.

OPH is dual-licensed: its software, including the Lean development and the model code, is Apache-2.0, while its papers, book, documentation, figures, data and ledgers are CC BY-NC-SA 4.0 [FloatingPragma, 2026]. This package therefore reimplements the software behaviour with attribution and reads no data or ledger from OPH. The carrier adjacency is the

clearest case: it is *derived* from OPH's twenty oriented faces and then checked against them, rather than transcribed from any table, and no OPH data file is read at run time.

FEP_Formal is CC BY 4.0 and is cited by DOI and by topic identifier [Friedman, 2026b]. The catalogue is read through its machine-readable metadata (`config/catalogue_metadata.yaml`), which is the schema-2 roster sealed at `fep-001` through `fep-168`; the generated projection `config/topics.yaml` is never authored or edited, because FEP_Formal declares it a projection and regenerates it.

QuadMath is Apache-2.0 [Friedman, 2025]. The constants this package needs are reimplemented and the source is cited by symbol: the neighbour moves, the embedding, the shell formula and the tetravolume convention. This paper quotes no QuadMath prose.

Two corrections in the provenance record are worth reporting, because both were caught by checking rather than by care. An earlier draft of this package attributed the carrier table to a Lean file that does not contain it; the attribution was false and the table was replaced by a derivation. And an earlier draft cited a QuadMath commit that had been superseded; the live checkout had moved, and the pin was updated. Both are recorded in `docs/PROVENANCE.md`. A pin is a point-in-time reading, and the discipline that matters is that the reading is re-done rather than remembered.

5.4 Why exactness, not agreement

It would be easier to report that three literatures "converge". The registry does not do that, for a reason that sec. 7 makes concrete: two programmes can agree on a number while disagreeing on the object the number is about. Existence without reachability Proposition 20 is the clearest example. Both programmes can be right that an equilibrium exists, and both can be right about its value, while one of them is wrong to infer that a trajectory reaches it. Agreement on the value would have hidden the disagreement about the dynamics.

The registry therefore distinguishes *what is computed* from *what is claimed about it*, and the statuses are assigned to claims. This is why the paper reports more disagreements than a synthesis-oriented reading would, and why the disagreements carry the same weight as the agreements.

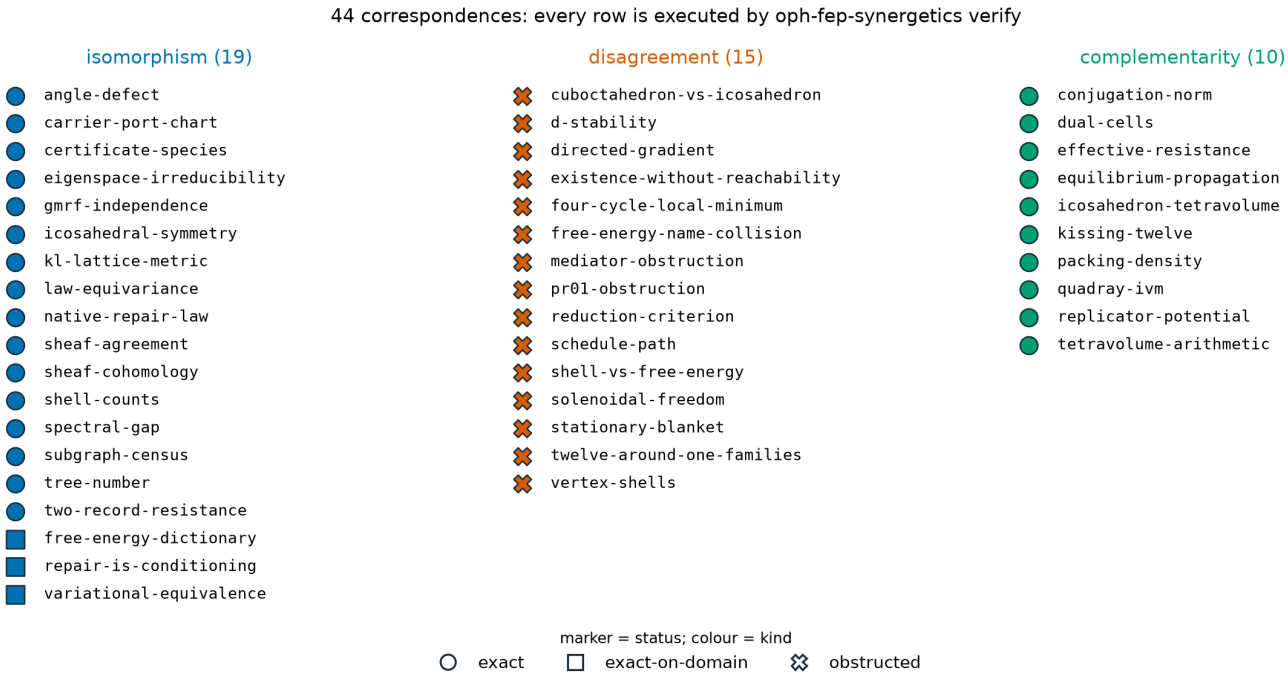


Figure 7: The registry as a matrix. Each row is one correspondence, coloured by kind (isomorphism, disagreement, complementarity) and marked by status (exact, exact-on-domain, obstructed). The figure is drawn from the same registry object that `oph-fep-synergetics verify` executes, so it cannot show an entry the probes do not carry. Generated by `scripts/make_figures.py` from `analysis/registry.py`.

6 Agreement: the identifications each pairwise scope survives

The registry records 19 isomorphisms across the three pairwise scopes. This section states each one, gives the exact values the probe reports, and says what the identification does *not* cover. fig. 7 shows the whole registry at a glance, and fig. 8 shows the same registry split by the pair of programmes each claim relates.

6.1 The port chart is a consequence, not a transcription

Proposition 1 is exact in the strongest sense available: the derivation returns 12 ports, 30 seams and 20 faces; every degree is 5; the twenty triangles of the derived graph are exactly the twenty oriented faces; and the derived adjacency equals the declared adjacency. The probe reports all six facts separately, so a failure of any one of them is visible rather than masked by the conjunction.

This matters for a reason that is methodological rather than mathematical. A published table of adjacencies can be copied with a transposition and still produce a plausible graph. Deriving the graph from the faces, and then checking that its triangles reproduce the faces, closes the loop: a transposition anywhere in the source data would break the round trip. The same pattern is used wherever this package reads a table that has consequences.

6.2 The spectrum is closed-form

Proposition 2 gives the full spectrum. The probe reports the eigenvalues as `2.763932` three times, six five times, and $5+\sqrt{5} \approx 7.236068$ three times, with the zero eigenvalue once, and checks that the Laplacian really is $5I - A$ rather than a normalised variant.

The gap is the quantity that carries dynamical meaning. Normalising by the total degree,

$$\gamma \;=\; \frac{\lambda_1}{2|E|} \;=\; \frac{5-\sqrt{5}}{60} \;=\; 0.04606553, \tag{9}$$

gives a number that is invariant under rescaling and is the one that appears in the relaxation estimates below. The corresponding **repair chain** is the symmetric stochastic matrix

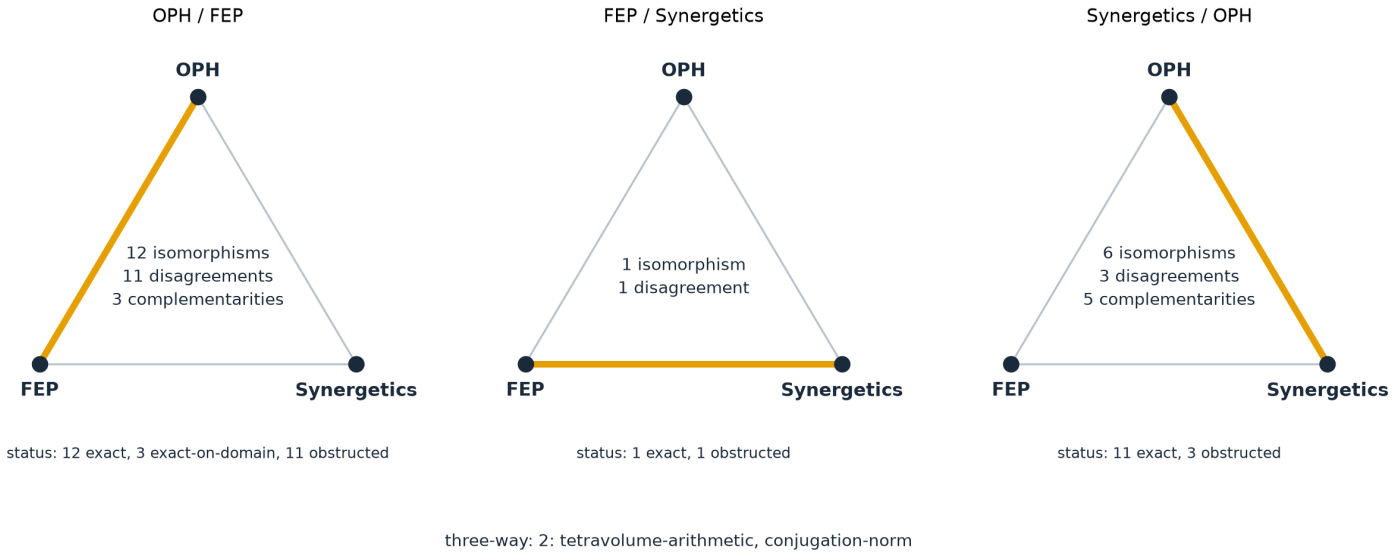


Figure 8: The three pairwise ledgers. Each triangle is one scope, named by the two programmes it relates; inside each triangle are that scope's counts by kind and its statuses, computed from the registry the command line executes. The panels are drawn from `analysis/registry.py` by `scripts/make_figures.py`, so a scope that gains or loses a claim changes its triangle.

$$P \;=\; I - \frac{L}{2|E|}, \tag{10}$$

whose rows sum to one, whose entries are non-negative because every degree is at most $2|E|$, and whose second eigenvalue is $1-\gamma = 0.9539345$ — the `certificate-species` correspondence, reported by the probe as a row-stochastic, symmetric, non-negative matrix with exactly that second eigenvalue and induced infinity norm 1. The chain of eq. 10 is the natural object behind the phrase "the shell mixes at the spectral gap": its mixing is governed by γ, and γ is a property of the carrier alone.

The chain is also what the integer rule does on average, and the probe checks that on the rule itself. Averaging eq. 1 over every seam and both coins, from each of the 78 configurations, returns $x - Lx/(2|E|)$ in exact rationals: the mean current across a seam is half its mismatch for either parity. OPH states the same identity as one gradient step of the seam-disagreement energy under its uniform calibration [FloatingPragma, 2026], so eq. 10 is derived from the law and the Laplacian is the law's own mean generator.

6.3 The shell is counted exactly

Definition 2 gives the count. The probe reports $|\Sigma_2| = \binom{13}{11} = 78$ total-two configurations and 66 binary ones, and checks the enumeration against the closed forms $\binom{13}{11}$ (stars and bars: two units of load over twelve ports) and $\binom{12}{2}$ (two occupied ports out of twelve), which share no code with it. The check is worth having because the enumerated set is the one that the repair census below partitions.

6.4 The native repair law is reproduced, not approximated

The `native-repair-law` correspondence reimplements OPH's rule on exact integers and checks it over all 4680 transitions of the 78-state shell. The rule itself is eq. 1; the closed form for the energy drop is $\Delta E = -(d^2 - (|d| \bmod 2))/4$, reported by the probe as a string so that the formula, and not merely a sample of its values, is part of the record.

The reimplementation is exact in the sense that matters: it is not a numerical approximation of OPH's rule but the same integer arithmetic, and the energy identity is checked rather than assumed. What the correspondence does *not* say is that OPH's rule is the right dynamics; that is an empirical question, and OPH's own status document records that no retained laboratory comparison selects a native record law [FloatingPragma, 2026].

Proposition 5. Let L be the carrier Laplacian partitioned into recorded ports o and free ports x, equip o with the prior in eq. 4, and let $x^*(o) = -L_{xx}^{-1} L_{xo}\, o$ be the harmonic extension of the records. The posterior has mean $x^*(o)$ and precision L_{xx}. At that posterior, the variational free energy takes the value $\mathcal{F}_{\mathrm{G}}(o) = -\ln p(o)$ [Mueller, 2026, theorem 7], with

$$S \;=\; L_{oo} - L_{ox} L_{xx}^{-1} L_{xo}, \qquad \mathcal{F}_{\mathrm{G}}(o) - \mathcal{F}_{\mathrm{G}}(o_0) \;=\; \tfrac{1}{2}(o^\top S\, o - o_0^\top S\, o_0) \;+\; \rho(o) - \rho(o_0). \tag{11}$$

The probe uses two antipodal carrier records with prior precision 0.5 and repeats the checks on a four-node chain. It computes the settled interior of eq. 11 three ways that share no linear solve. The harmonic extension solves the interior block. The constrained minimiser solves one saddle-point (KKT) system for $\min \frac{1}{2} z^\top L z$ subject to $z_o = o$ over all coordinates and a multiplier per record. The prior contributes a fixed term at fixed records, so the same constrained solution minimises the relative entropy of a mean shift at fixed joint precision. This is the constrained relative-entropy reading of OPH's premise A3. And the predictive-coding flow `perceive` reaches the same point in 143 iterations with residual 9.169439e-11, from every start tried. The probe also evaluates the free energy at the posterior directly, as energy minus entropy, and finds it equal to the surprisal: the divergence in eq. 3 has numerical residual 0 because the bound is tight at the posterior.

The boundary control clamps a single record on an oriented seam with an asymmetric spring. The energy is piecewise quadratic, with twice the stiffness for positive disagreement. Its unique minimiser is at zero disagreement, while numerical integration and a half-Gaussian calculation give a negative posterior mean. The equality of minimiser and posterior mean in Proposition 5 depends on the Gaussian assumption.

6.5 Each native repair is exact conditioning

The identifications above read one object in two vocabularies. This one relates the native law itself to a free-energy functional, and it is exact [Mueller, 2026, Mueller et al., 2026].

A repair of a seam conserves the load on the seam and touches no other port. The seam's total load together with every load off the seam is therefore the same before and after the repair. That pair is the datum the repair leaves visible, and the configurations that share it are its fibre.

Proposition 6. Let u be the uniform law on the 66 binary configurations and K_e the law of one native repair of the seam e under its fair coin. For every binary configuration x and every seam e, $K_e(x, \cdot)$ is u conditioned on the datum o of x at e. With $\pi(s, o) = u(s)$ for s in the fibre of o, $K_e(x, \cdot)$ is the unique minimiser of

$$\mathcal{F}[q] \;=\; \mathbb{E}_q[\ln q(s) - \ln \pi(s, o)] \tag{12}$$

over the laws q on the fibre, and the minimum is the surprisal $-\ln \pi(o)$ of the datum.

The probe compares the two sides of Proposition 6 in all 3960 cases, both orientations of every seam from every binary configuration, by routes that share no code: the integer rule on one side, the reference and the datum on the other. A seam that holds one unit has a fibre of two configurations and the repair resamples the unit's side with equal weights, which happens in 1200 cases; every other seam has a fibre of one. The surprisal is `log 33` in the first case and `log 66` in the second. Evaluated on eq. 12, a coin with any bias pays exactly its divergence from the fair coin above that minimum, and a rule that always waits or always swaps pays `log 2`.

Because K_e is a conditional expectation of u, every law p on the shell obeys $D(p \,\|\, u) = D(p \,\|\, pK_e) + D(pK_e \,\|\, u)$. Each repair lowers the relative entropy to the reference by exactly $D(p \,\|\, pK_e)$, which the probe checks on a mixed state for every seam. OPH states both facts for the binary shell [FloatingPragma, 2026, Mueller et al., 2026].

The status is `exact-on-domain`, and the probe asserts the boundary. With the uniform law on all 78 configurations as reference the identity fails at the doubled configurations, on the 60 seams that meet a doubled port out of 360 off-shell cases: the repair moves one unit across with certainty, and conditioning would spread the weight over three configurations.

In the FEP's vocabulary each native repair is a perception step whose recognition density is the exact posterior, with the uniform reference as prior and the repaired datum as observation, so the bound of eq. 3 is tight at every step. The functional each step minimises is eq. 12. It is a different object from the load energy of eq. 2, which sec. 7.1 shows to be constant along the binary shell while every step there is exact inference. Registered as `repair-is-conditioning`.

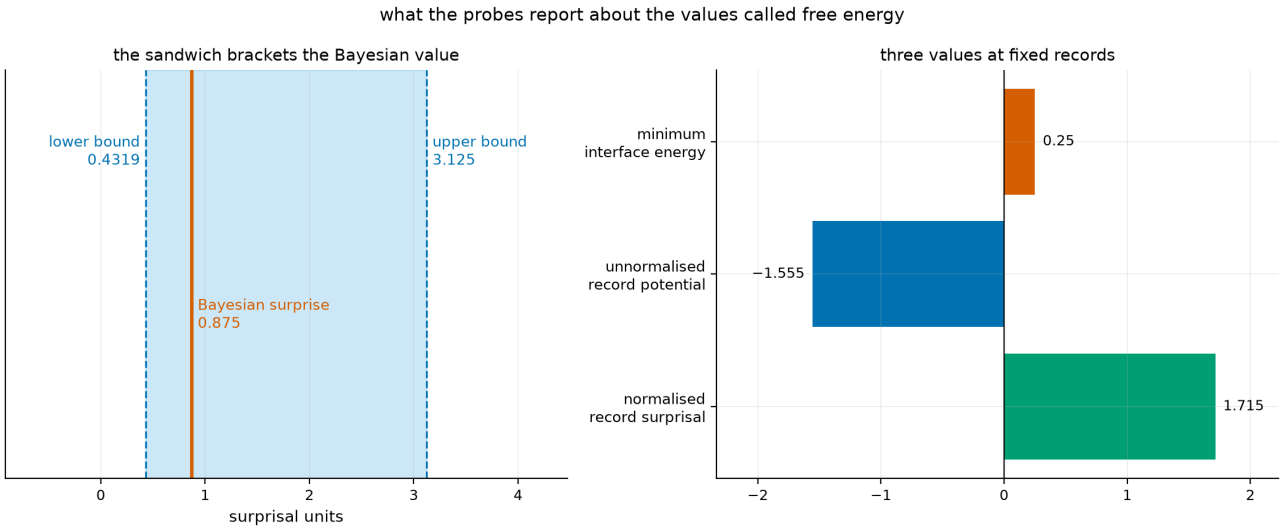


Figure 9: Two panels read from the executed probes. Left: the sandwich interval with its lower bound 0.4318644 and upper bound 3.125, and the Bayesian surprise 0.875 marked inside it. Right: three quantities at the same records: minimum interface energy 0.25, unnormalised record potential -1.555415, and normalised record surprisal 1.714912. Generated by `scripts/make_figures.py` from `core/free_energy.py` and `core/controls.py`.

6.6 The free-energy dictionary has a precise scope

Three quantities are routinely called "surprisal", and the source literature distinguishes five: (numerical, bayesian, surprisal, critic, meaningful) [Mueller, 2026]. In the linear-Gaussian model this package computes three of them, and tbl. 5 reports what happens. The registry entry is `free-energy-dictionary`.

Table 5: Three surprises in the linear-Gaussian carrier probe. The residual norm and Bayesian surprise describe a change of records. Record surprisal uses the new records alone. The sandwich bound brackets the Bayesian value [Mueller, 2026, theorem 7 and table 7].

Quantity	Definition	Value in the probe model
numerical surprise	residual norm $\|g\|$ at the old rest	2.5
Bayesian surprise	$\frac{1}{2} g^\top L_{xx}^{-1} g$	0.875
record surprisal	$-\ln p(o)$ under the proper joint model	3.994912
variational free energy	eq. 3 at the posterior	3.994912

The probe reports a sandwich with lower bound 0.4318644 and upper bound 3.125, and the Bayesian value 0.875 lies inside it. The energy drop at the new records and the divergence between posteriors give the same value by independent routes. The variational free energy equals record surprisal at the posterior and exceeds it by the divergence from the posterior away from that optimum.

The asymmetric seam gives a check outside this domain. Ground one port and read the other with a symmetric record prior. Records of opposite sign and equal magnitude have different surprisals, because the prior and the normaliser cancel in their difference and the seam energies do not agree. The centred quadratic record formula cannot represent this difference.

6.7 A sheaf computes the same Laplacian

The scalar carrier construction instantiates the cellular sheaf formulation of agreement [Mueller, 2026, sec. 7.2 and theorem 7].

Proposition 7. Give every port the stalk $\mathbb{R}$ and every seam the identity restriction. The resulting cellular sheaf on K has 30 edges, Laplacian equal to the carrier Laplacian, one-dimensional space of global sections (the constants), and injective record maps at every port.

The probe reports all of this, and it reports two negative controls: a chain sheaf with one record has a one-dimensional space of global sections, and a chain sheaf with no record has none. The controls matter because a sheaf whose global sections are one-dimensional for every choice of records would not be saying anything about the carrier. Registered as `sheaf-agreement`.

The sheaf formulation is the one that generalises. A scalar identity sheaf is the simplest case; the same construction with non-identity restrictions is how the FEP's precision structure would enter, and the harmonic-extension identity of Proposition 5 is the same computation written in sheaf language [Hansen and Ghrist, 2019, Robinson, 2014]. The agreement reported here is therefore not a coincidence of two implementations but a statement that the carrier's Laplacian is the coboundary Laplacian of a sheaf, which is the bridge [Friedman, 2026c] proposed.

6.8 The carrier counts its own spanning trees

Proposition 8. Delete any row and the matching column of the carrier Laplacian. The determinant of the remaining 11×11 matrix is an integer, and by Kirchhoff's matrix-tree theorem [Kirchhoff, 1847] that integer is the number of spanning trees of the seam graph:

$$\tau(K) \;=\; 5184000 \;=\; \frac{1}{12}\prod_{i=2}^{12}\lambda_i. \tag{13}$$

The probe reports the determinant computed in exact rational arithmetic, and, separately, the product of the eleven nonzero eigenvalues computed in floating point: the first is 5184000, the second agrees with it to nine digits. The two computations are not redundant. The eigenvalues include the surds $5 \pm \sqrt{5}$ three times each, so an exact integer arising from a product of irrationals is a statement about the arithmetic and not about the sampling; the floating-point product is reported next to it because the disagreement between the two is the honest error bar on the spectral route.

The count is not decoration. One determinant, two readings: in OPH's the integer counts the seam sets that connect every port without a cycle; read as a Gaussian precision with one port pinned (the gauge that makes it proper), the same determinant normalises the linear-Gaussian interface integral the FEP dictionary factorises through. Either way the carrier's spanning trees are a finite, exactly known family, so any claim about the existence of an agreement configuration can be phrased as a claim about a member of a set of known size. sec. 7.7 is the obstruction that shows why the size of that set does not by itself settle reachability.

6.9 The Gaussian reading makes the seam graph the independence graph

Use $L + I/n$ as the precision of a proper Gaussian field on the n carrier ports. The positive diagonal shift grounds the constant mode and leaves the off-diagonal entries unchanged. The precision's zeros determine conditional independence [Dempster, 1972, Rue and Held, 2005]: two ports are independent given the rest exactly when their precision entry vanishes, which here happens exactly when they are not joined by a seam, so conditional dependence lives exactly on the seams. The probe reports the independence pattern as a 12×12 matrix over all 60 ordered pairs of distinct ports, checks that it equals the adjacency pattern, and checks that the shifted precision is positive definite.

Every seam's pairwise precision is -1. A port's Markov blanket consists of its 5 neighbours. For the separate intrinsic field centred to sum to zero, the covariance is L^+ and each port's variance is 0.1944444, exactly 7/36. Vertex transitivity gives this value by dividing the reciprocal spectrum sum by n. The probe computes the sum over the rationals as $\mathrm{tr}((L + J/n)^{-1}) - 1$, where J is the all-ones matrix.

Conditioning the proper Gaussian on all other ports gives the graph result. For the centred intrinsic field the same conditioning fixes the sum of the remaining pair, including for nonseams. sec. 7.3 separately tests whether a blanket in a stationary density constrains the dynamics.

6.10 Two cohomology dimensions, one global section

Proposition 9. Give every port the stalk $\mathbb{R}$ and every seam the identity restriction, and let δ^0 be the resulting coboundary on the seam graph. Then $\dim H^0 = 1$ (the constants), $\dim H^1 = 19$, and δ^0 has rank 11, so the Euler characteristic of the graph is -18. Adding the twenty faces as two-cells, with δ^1 the signed face-seam incidence, δ^1 has rank 19: the surface has Betti numbers (1, 0, 1) and Euler characteristic 2, and OPH's oriented faces sum to a fundamental cycle.

The probe reports both coboundaries' shapes and ranks in exact arithmetic, all the cohomology dimensions, both Euler characteristics, the check that $\delta^1\delta^0 = 0$, and the dimensions of the same quantities for a chain sheaf used as a control.

The two numbers have concrete readings, which is the reason for reporting them separately rather than as one identity. The global sections are the assignments of equal values to adjacent ports, so $\dim H^0 = 1$ says that the only way for every seam to agree is for every port to carry the same value: the agreement is a constant. The cohomology dimension $\dim H^1 = 19$ measures seam assignments modulo coboundaries of port assignments. Its value is the cycle rank of the seam graph, $|E| - |V| + 1 = 30 - 12 + 1$. Every disagreement that a port assignment actually produces lies in the image of δ^0. Both dimensions are forced by the graph [Hansen and Ghrist, 2019, Ghrist, 2014].

The second half of Proposition 9 reconciles two numbers the paper uses. The graph's Euler characteristic is -18; the surface's, which the angle-defect count of Proposition 13 reaches through Gauss-Bonnet, is 2. The difference is the faces: the face-seam incidence has rank 19, equal to the cycle rank, so the face boundaries span the graph's cycle space and no first cohomology survives on the sphere. The oriented faces sum to a cycle – every seam is traversed once in each direction. This checks the coherence of the declared orientation used by the rotation and reflection count Proposition 10.

6.11 The symmetry group closes the census

Proposition 10. The automorphism group of the carrier has order 120, is closed under composition, and acts transitively on the 12 ports, the 30 seams and the 20 faces. It splits into 60 rotations and 60 reflections, and the Laplacian eigenspaces of dimensions (3, 3, 5) are irreducible under it. Across all group elements and all 78 total-two configurations, the multiset of descent outcomes takes 3 values, on 4 orbits of configurations.

The probe reports each part separately: the group order from an exhaustive backtracking search, closure under composition, the orbit decomposition of ports, seams and faces, the split into rotations and reflections, the orbit ranks and commutant dimensions of the three nontrivial eigenspaces against their dimensions, and the equivariance of the descent law over the full product of 120 group elements and 78 configurations.

Three readings follow, and they are the reason this correspondence is in the registry rather than in an appendix. First, the symmetry is a symmetry of the *object*, so any claim about the carrier that is not group-invariant is a claim about a labelling. Second, the eigenspaces being irreducible means the multiplicities (3, 3, 5) are forced: they are the dimensions of the icosahedral group's representations, so no perturbation that keeps the symmetry can change the multiplicity pattern. The eigenvalues are not forced: the permutation representation is multiplicity-free, so every invariant symmetric matrix has these eigenspaces, each with its own value. Third, and most useful for this paper, the repair law is equivariant transition by transition: for every group element, configuration, oriented seam and coin, repairing the relabelled configuration on the relabelled seam gives the relabelled result, so the multiset of outcomes is preserved, and the probe finds no witness that would break it. The census numbers in sec. 7.1 are therefore invariants, and the 4 orbits are the right unit of analysis. The registry carries this section as three entries: `icosahedral-symmetry`, `eigenspace-irreducibility` and `law-equivarianc e`.

The rotation and reflection counts require the orientation of the faces, and that detail is a correction worth reporting. Testing orientation by the set of directed edges of a face fails on a closed surface, because such a set already contains every edge in both directions; the test used here compares the cyclic order of each face, rotated so that its smallest port leads, and only then does it separate 60 rotations from 60 reflections.

6.12 Information cost is the synergetic metric over two

Proposition 11. For two Gaussians of equal covariance Σ centred at the origin and at a lattice site z, the Kullback–Leibler divergence is half the squared Mahalanobis norm of the separation; with $\Sigma = I$ in the default embedding,

$$D_{\mathrm{KL}}(\mathcal{N}(0, I) \,\|\, \mathcal{N}(z, I)) \;=\; \tfrac{1}{2}\|z\|^2, \tag{14}$$

and the IVM's first neighbour shell sits at squared norm 8, so one step costs 4 nats and the sites $k\,m$ along a neighbour move m cost 4, 16, 36 and 64 nats for $k = 1, \ldots, 4$, that is $4k^2$.

The probe reports the divergence for each of the twelve neighbour moves, the squared distance of a move, and the costs of the sites $k\,m$ for the first four multiples [Kullback and Leibler, 1951].

This is the shortest of the identifications and the one with the widest reach, because it is the only place in the registry where the FEP's own currency and Synergetics' own metric are the same function. The lattice supplies the distances; the divergence turns them into costs; and because every squared distance between lattice sites is a multiple of eight in this embedding, every cost is an integer number of nats, a multiple of four. The number four is a statement about the unit of length, not about the lattice: rescaling the covariance rescales every cost by the same factor, and with the covariance equal to the squared prime

vector one step costs half a nat. What the identification fixes is the ratio of costs, which is the ratio of squared distances. It also fixes a convention that the paper uses everywhere else: a "one-step cost" is a divergence, not an energy, and the two differ by the factor of two that eq. 14 makes explicit.

6.13 The carrier's subgraphs are the solid's own counts

Proposition 12. Counting the seam graph's subgraphs by exhaustion returns 20 triangles, 12 induced (chordless) five-cycles, 125 perfect matchings and 1280 Hamiltonian cycles counted as undirected edge sets, and the first of those is exactly the number of faces the port chart was derived from.

The probe enumerates rather than quotes: every three-vertex subset for the triangles, every five-vertex subset for the pentagons, and a memoized recursion for the matchings and the Hamiltonian cycles, all from the adjacency matrix alone. The triangle count is where two derivations meet. The carrier's faces were *derived* from OPH's oriented base faces in sec. 6.1, and the census then *rediscovers* 20 triangles in the graph that derivation produced. A count that agreed by construction would prove nothing; this one is computed from the adjacency and checked against the face list afterwards.

The induced five-cycles are the links of the twelve ports, one around each, and so they are the twelve pentagonal faces of the dual dodecahedron, which is the first place in the paper where the dodecahedron appears without being named. The perfect matchings and the Hamiltonian cycles have no counterpart in any of the three programmes, and that is the reason to report them: they are properties of the object all three are about, available to anyone who can read its adjacency.

6.14 Curvature is exact in units of pi

Proposition 13. Five equilateral triangles meet at every port, so each port carries an angle defect of 1/3 pi and the twelve ports carry 4 pi in total, which is $2\pi\chi$ for a triangulated sphere: Descartes' theorem on the total angular defect, the combinatorial form of Gauss-Bonnet, read off the face list [Federico, 1982].

The probe computes each defect as twice pi minus the incident faces times pi over three and returns it as an exact rational multiple of pi rather than as a decimal: 1/3 at each port, 4 in total, against the surface Euler characteristic 2 that the cohomology of Proposition 9 reaches from the other direction. OPH's derived chart is the icosahedron's triangulation, so the angular-defect accounting Synergetics supplies for that solid applies unchanged: the vertex figure the accounting measures is the very five-face figure every port carries. The identity is the reason twelve five-fold vertices close into a sphere rather than a dish, and it is exact for the same reason the tree number is: rational quantities over a finite complex. Registered as `angle-defect`.

fig. 10 draws this section and the two that follow it: the resistance ladder, the shells around a port, the census (Proposition 12), the defect (Proposition 13), and the dual pair.

6.15 What the agreements do not say

One identification relates OPH's *dynamics* to a free-energy *functional*: on the binary shell each native repair minimises eq. 12 (Proposition 6). It holds step by step on that shell. It leaves the load energy of eq. 2 what it was, and it says nothing off the shell. Several of the other identifications are statements about counting, and most of the rest are statements about the carrier, its spectrum, its repair rule as an integer map, the Gaussian free energy on it, and the sheaf whose Laplacian it is. Every one of those is a statement about a finite object that both programmes can be given.

The remaining identifications are structural rather than numerical, and the paper reports them with the same care: a symmetry group of order 120 is exact arithmetic, a spanning-tree number is an exact integer, and a cohomology dimension is an exact rank. What none of them supplies is a claim that either programme's *learning* dynamics is the other's.

The next section reports the places where an identification fails, and most of them fail for one reason: the authors of each programme attach a *dynamical* claim to that shared object, and the dynamical claims do not agree.

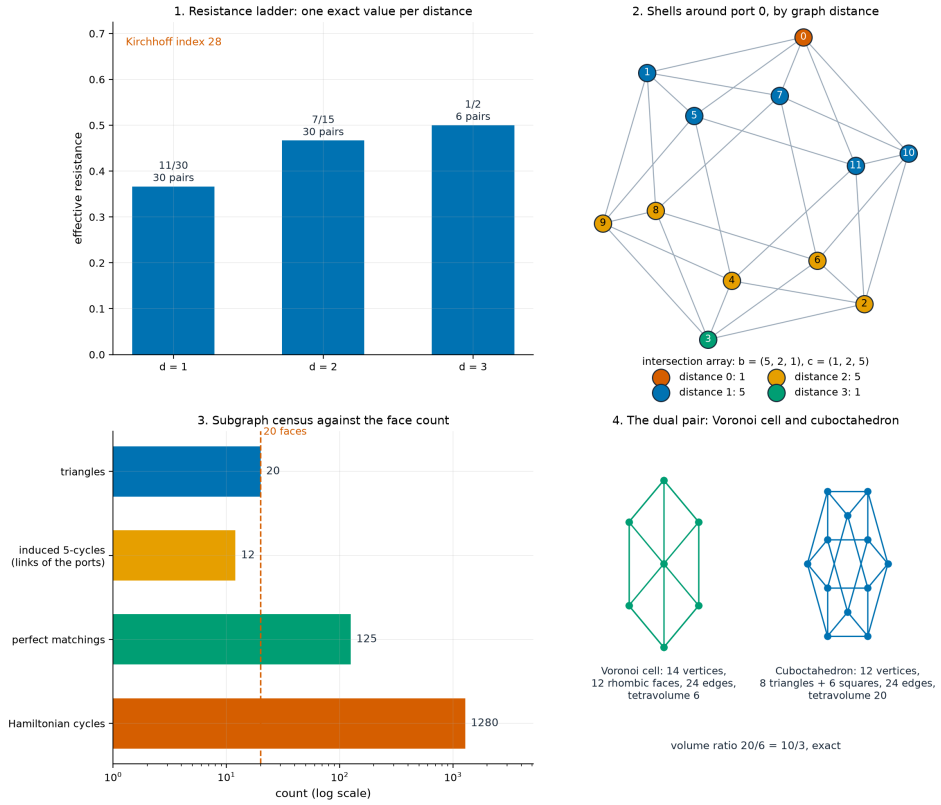


Figure 10: The carrier read as a network. Panel one gives the exact resistance ladder between port pairs with the Kirchhoff index; panel two colours the twelve ports by their graph distance from one port and annotates the intersection array; panel three counts the subgraphs; panel four compares the twelve-around-one cell with its dual, whose counts and tetravolumes are read from the geometry package. Every number is computed from the executed package at draw time rather than transcribed.

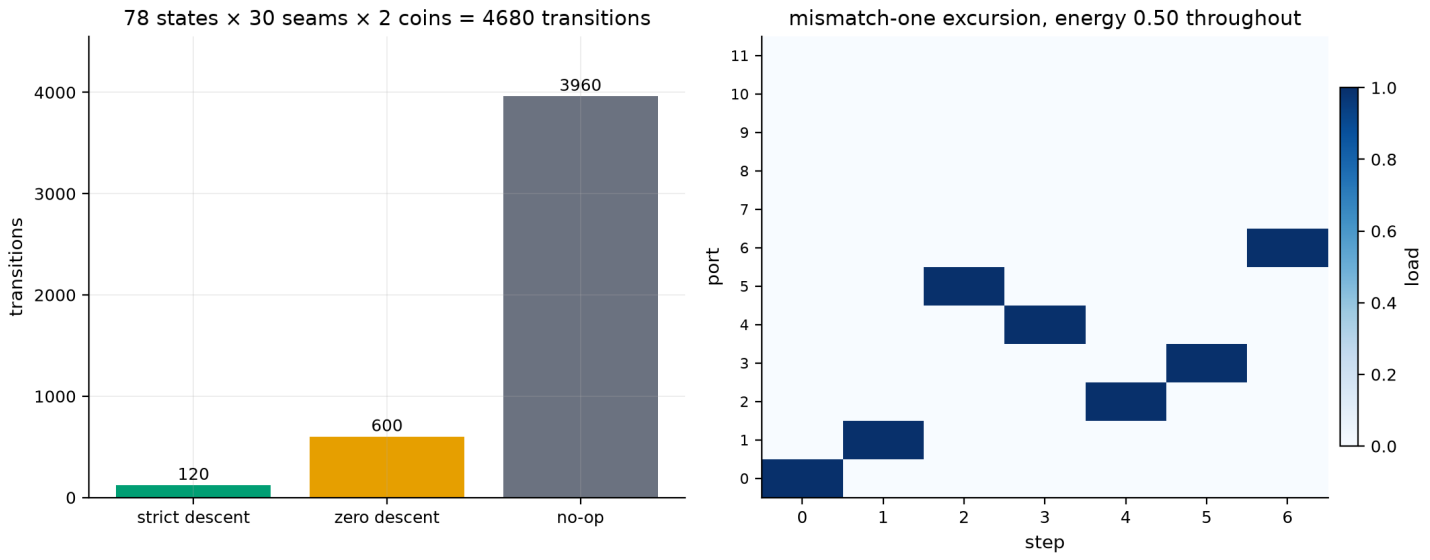


Figure 11: The descent census and a mismatch-one excursion. Left: the 4680 transitions of the shell, partitioned into 120 strict descents, 600 zero descents and 3960 no-ops. Right: a one-unit excursion around the carrier through distinct configurations while the quadratic energy stays at 0.5, so the trajectory has no descent to offer and no unique limit. Generated by `scripts/make_figures.py` from `core/controls.py::gated_descent_census`.

7 Disagreement: the obstructions, each stated exactly

An obstruction is a result. Each of the 15 claims below was proposed as an identification, and each fails in a way that can be stated exactly. The section is ordered by how much the failure costs a synthesis: the first distinguishes confluence from termination for OPH's native rule, the next two block the identification of "free energy", the remainder block dynamical identifications that the literature makes routinely, and the last two block identifications that are made by counting rather than by dynamics.

7.1 The native law does not terminate

OPH's PR-01 distinguishes its native seam rule from the integer and transactional contracts that carry its consensus theorems [FloatingPragma, 2026]. In the Lean library, `demoCarrier_not_confluent` and `demoCarrier_terminates` concern a separate Boolean copy-repair example. The native rule instead fails termination on the carrier's total-load-two shell. At mismatch one a native attempt waits or swaps the odd unit; the swap changes the state at constant load energy [Mueller, 2026, sec. 6.2]. Registered as `pr01-obstruction`.

Proposition 14. Over the 78 configurations of Σ_2, the 30 seams and the two coins, the native rule has 4680 transitions. Of these, 120 strictly lower eq. 2, 600 leave it unchanged, and 3960 leave the configuration unchanged. In particular the zero-descent transitions are not rare: they outnumber the strict descents, and the multiplicities of the native transitions take exactly the values (1, 2, 50, 52).

The mechanism is eq. 1 itself, and the energy identity is Proposition 3. At $|d| = 1$ the parity correction absorbs the whole of the move: coin zero's current is 1 and coin one's is 0, so one coin performs a swap at constant energy and the other does nothing at all. The probe reports both currents and both energy decreases, which are 0 and 0. fig. 11 shows the census and an excursion.

The same draws fix the two probabilities the source states for the configuration with one unit on each of two adjacent ports [Mueller, 2026]. One attempt is a uniform seam and a fair coin. The configuration stays where it is with probability 13/15 and moves to each of 8 neighbouring configurations with probability 1/60, and every draw leaves eq. 2 unchanged. Two transitions with the same energy decrease differ in surprisal, so no coefficient converts the path surprisal of the native law into its energy decrease. OPH's model states the kernel and both values [FloatingPragma, 2026]; the probe enumerates the draws and checks the result against a count of the seams that meet exactly one of the two occupied ports.

Proposition 15. Count only state-changing repairs as rewrite steps. On the whole shell, the ungated relation has 0 normal forms and admits a cycle. The binary configurations form one closed, strongly connected class reachable from every state,

so any two descendants of the same state can reach a common successor: the relation is confluent but does not terminate. Under the broken-seam gate, every step strictly lowers load energy. The gated relation terminates, with the 66 binary states as normal forms. Each doubled state reaches 5 distinct normal forms, so the gated relation is not confluent.

The state graph in Proposition 15 concerns individual paths. Under a uniform seam and fair coin, the binary-shell attempt kernel includes the waits. Its transition-count matrix is symmetric with all row and column totals equal to the number of draws. The uniform law is stationary, connectivity gives its uniqueness, and the computed spectral gap equals the port gap in Proposition 2. Each single-seam kernel is a conditional expectation (Proposition 6); the mixture also preserves the uniform law. Data processing makes relative entropy to that law nonincreasing for every initial binary-shell distribution. The probe separately checks a trajectory from a point mass and the spectral bound on chi-square divergence. This bound does not assign a universal decay rate to relative entropy. Thus a path can keep its load energy constant while the ensemble loses relative entropy.

7.2 Three distinct values at fixed records

On the carrier the minimum interface energy $\min_x E(x, o)$ is 0.25. The unnormalised record potential $-\ln \int \exp(-E(x, o))\, dx$ is -1.555415. Their difference -1.805415 equals the interior Gaussian term $\frac{1}{2} \ln\det L_{xx} - \frac{d_x}{2} \ln(2\pi)$, computed independently as -1.805415.

For the normalised model, record surprisal and variational free energy at the posterior both equal 1.714912. This value includes the record prior energy and the record normalisation term 1.432412 from eq. 4. The interior term cancels against the corresponding term in the joint normaliser [Mueller, 2026, theorem 7]. Two chain controls with identical Schur complements and the same prior give identical surprises despite different interior determinants and unnormalised potentials. Registered as `free-energy-name-collision`.

7.3 A stationary blanket does not bound the dynamics

This control follows Mueller's proposition using the three-state blanket example of Da Costa et al. [Mueller, 2026, proposition 11; Da Costa et al., 2021].

Proposition 16. Order the state as exterior η, blanket b and interior μ, let the precision be $H = \left(\begin{smallmatrix} 2 & 1 & 0 \\ 1 & 2 & 1 \\ 0 & 1 & 2 \end{smallmatrix}\right)$, so that $H_{\mu\eta} = 0$, and let Q be antisymmetric with $Q_{\mu\eta} = q$. The diffusion $\mathrm{d}z = -(I - Q)Hz\,\mathrm{d}t + \sqrt{2}\,\mathrm{d}W$ has stationary law $\mathcal{N}(0, H^{-1})$ for every q, which satisfies eq. 5 exactly. Its interior drift is $\dot{\mu} = 2q\,\eta + (q - 1)\,b - 2\mu$, which at $q = 0.75$ has coefficients (1.5, -0.25, -2) on (η, b, μ), so two states with equal blanket and interior values move differently whenever their exteriors differ, with cross-drift difference 1.5.

The stationary law factorises; the dynamics does not. The conditional independence of eq. 5 is a property of a distribution, and a system can have it at stationarity while every trajectory through the state space mixes the interior and the exterior. The probe reports the factorisation and the coupling in the same mapping, so the reader cannot take the first without also seeing the second.

This is the disagreement that the critical literature presses [Bruineberg et al., 2022, Biehl et al., 2021, Aguilera et al., 2022], and the probe says it precisely: the blanket is real as a statistical statement and insufficient as a dynamical one. A synthesis that needs a boundary to *do* something — to shield, to persist, to constitute an agent — needs an additional condition on the drift, and that condition is not implied by eq. 5.

7.4 Stationary blankets leave entropy production free

Mueller's entropy-production control uses a family of diffusions with a common stationary law, following work on nonreversible Gaussian diffusions [Mueller, 2026, proposition 9; Hwang et al., 1993; Lelièvre et al., 2013].

Proposition 17. For $\mathrm{d}x = -(\Gamma - Q)Hx\,\mathrm{d}t + \sqrt{2\Gamma}\,\mathrm{d}W$ with Γ, H positive definite and Q antisymmetric, the law $\mathcal{N}(0, H^{-1})$ is stationary for every Q and the entropy production rate is $\mathrm{tr}(Q^{\top}\Gamma^{-1}QH)$. In two dimensions with $\Gamma = H = I$ and $Q = q\left(\begin{smallmatrix} 0 & 1 \\ -1 & 0 \end{smallmatrix}\right)$ the drift has eigenvalues $-1 \pm iq$ and the entropy production is $2q^2$: (0, 0.5, 4.5) at $q \in (0, 0.5, 1.5)$. Stationarity therefore does not fix the entropy production, and cannot be used to infer it.

The solenoidal component of the drift — the part that circulates without changing the stationary density — is invisible to the stationary law and fully visible in the entropy production. fig. 12 draws both panels.

This is the sharpest of the disagreements, because it is a statement about what a stationary-blanket argument can and cannot conclude. The dissipative structure is constrained; the circulating structure is not [Ao, 2004, Seifert, 2012, Godrèche and

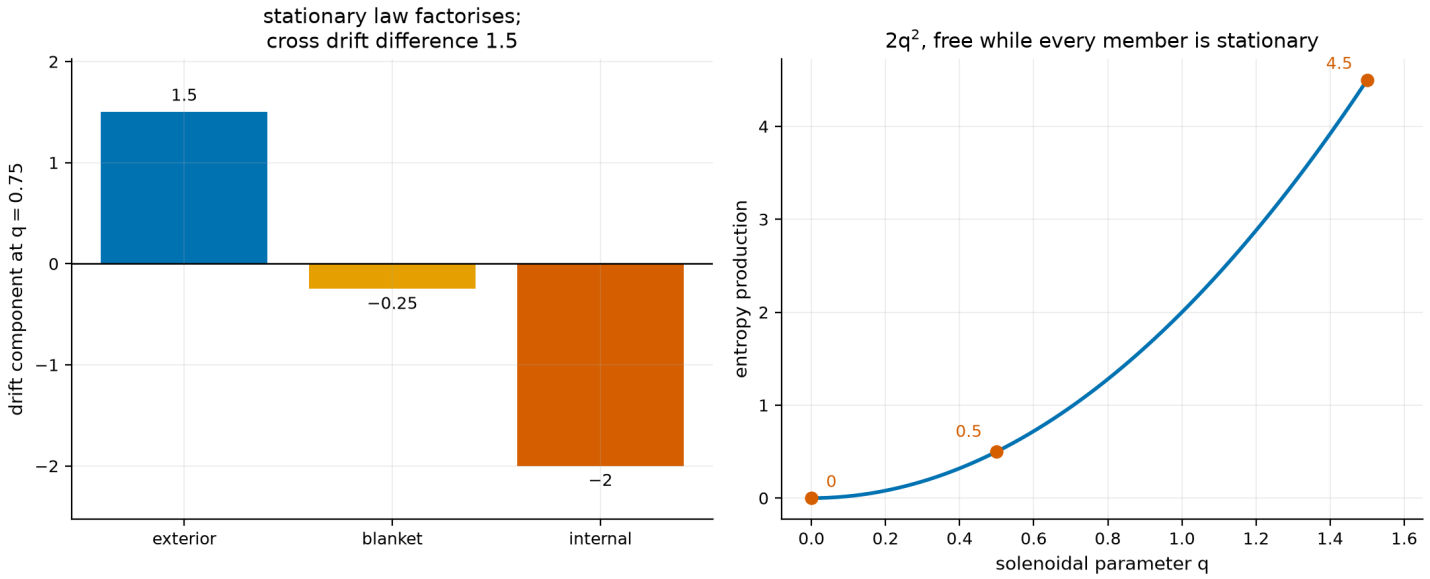


Figure 12: Stationary blankets and their freedom. Left: the three drift components at $q = 0.75$, showing that the drift couples the exterior and the interior even though the stationary law factorises. Right: entropy production against the solenoidal parameter q, which is $2q^2$ and therefore free, while every member of the family is stationary. Generated by `scripts/make_figures.py` from `core/controls.py::blanket_dynamics_check` and `solenoidal_check`.

Luck, 2019]. A free energy argument that works only from stationarity therefore cannot reach the thermodynamic quantities that the solenoidal part controls. Registered as `solenoidal-freedom`.

7.5 Stability is not generic in the coupling

Definition 5. A real matrix A is **stable** when every eigenvalue has negative real part, and **D-stable** when DA is stable for every positive diagonal matrix D [Arrow and McManus, 1958]. A positive diagonal D is a choice of local repair gains that leaves the rest point $DAx = 0$ where it was.

Proposition 18. Let $A = \left(\begin{smallmatrix} -1 & 2 & 0 \\ 2 & -1 & 3 \\ 0 & -3 & -1 \end{smallmatrix}\right)$ be Mueller's stable three-node control matrix [Mueller, 2026, sec. 4.1 and proposition 10], and let $D_k = \mathrm{diag}(k, 1, 1)$. The family $D_k A$ has characteristic polynomial $z^3 + (k+2)z^2 + (10-2k)z + 6k$, and its Routh first column is

$$\left(1, \quad k+2, \quad \frac{2\,(10-k^2)}{k+2}, \quad 6k\right), \tag{15}$$

so for $k > 0$ every root has negative real part exactly when $k < \sqrt{10} \approx 3.162278$. At $k = 4$ the column is `(1, 6, -2, 24)`, whose two sign changes certify 2 right-half-plane roots. A is stable and not D-stable.

The eigenvalues at $k = 4$ are -6.288814 and 0.144407 with imaginary part ± 1.948191: the complex pair has positive real part, and the system spirals out.

What is lost is a free-energy form. A linear law admits the Helmholtz decomposition $A = -(\Gamma - Q)H$ with Γ, H positive definite and Q antisymmetric – the Ornstein-Uhlenbeck form whose stationary density is $\propto \exp(-\frac{1}{2}x^\top H x)$ – exactly when A is stable: with $\Gamma = I$ the Lyapunov equation $AP + PA^\top = -2I$ gives $H = P^{-1}$ and $Q = \frac{1}{2}(AP - PA^\top)$ [Khalil, 2002]. For the unscaled A the source's certificate is exact: P is positive definite with $\det P = 4.259259$, the residual of the Lyapunov equation is 2.531698e-15, and Q is antisymmetric [Mueller, 2026]. At $k = 4$ no positive-definite solution exists, because $D_4 A$ is unstable, so one positive local gain removes the form without moving the rest. Mueller embeds the control in a nonlinear field [Mueller, 2026, proposition 10]. With $W = 4(A+I)$ and a logistic activation, the bounded neural field $f(v) = -v + W\sigma(v) + b$ with $b = -W(\frac{1}{2}, \frac{1}{2}, \frac{1}{2})^\top$ has $f(0) = 0$ and Jacobian exactly A at the origin, which the probe confirms with zero error. The obstruction is therefore not that the algebra fails. It is that stability is a property of a point in a parameter space, and the identification of a repair rule with a stable descent needs D-stability (Definition 5), every admissible gain on the stable side. Here the stable region is $k < \sqrt{10}$, which is not the whole admissible range. Registered as `d-stability`.

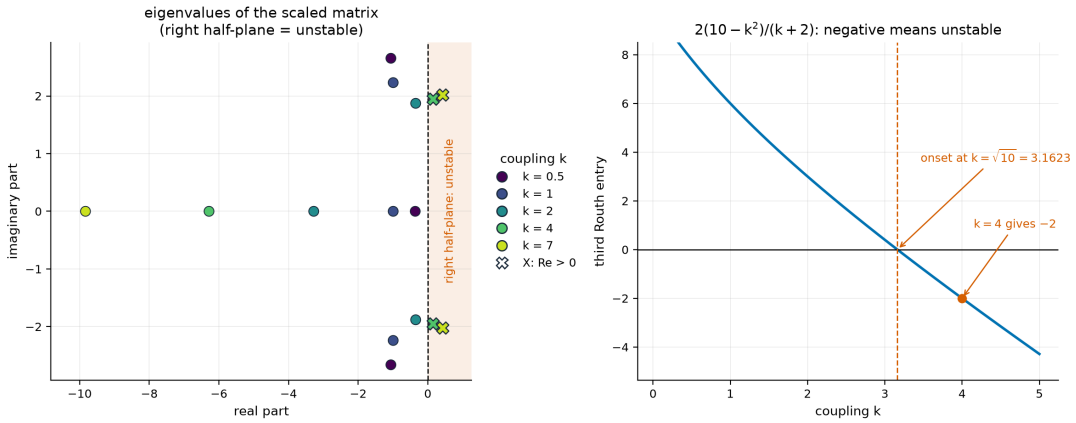


Figure 13: D-stability. Left: the eigenvalue locus of $D_k A$ in the complex plane for $k \in (0.5, 1, 2, 4, 7)$, with the imaginary axis drawn; the pair that crosses into the right half plane is marked. Right: the third Routh entry $2(10 - k^2)/(k + 2)$ of eq. 15, which changes sign at $k = \sqrt{10}$ and is -2 at $k = 4$. Generated by `scripts/make_figures.py` from `core/controls.py::d_stability_eigenvalues` and `routh_first_column`.

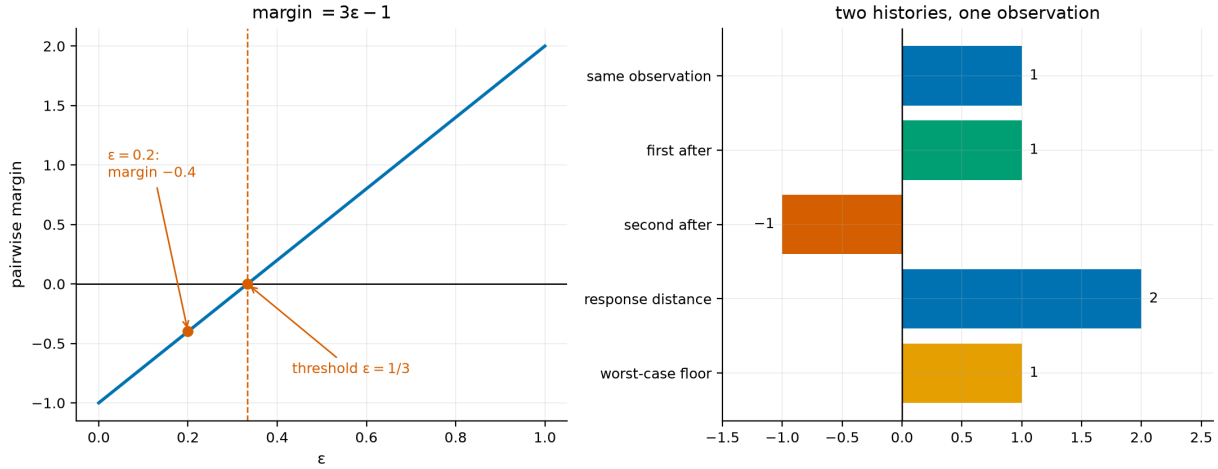


Figure 14: The mediator threshold. Left: the pairwise margin $3\varepsilon - 1$ against ε, -0.4 at $\varepsilon = 0.2$ and crossing zero at the threshold `0.3333333`. Right: the reduction error at and below the threshold, showing that the worst-case error floor is 1 while retaining the record is exact. Generated by `scripts/make_figures.py` from `core/controls.py::mediator_pairwise_margin` and `reduction_control`.

7.6 Reduction needs a threshold

The mediator model and the trace proof of the threshold come from Mueller [Mueller, 2026, proposition 8]. The probe here also constructs and checks the rank-one blocks at the threshold.

Proposition 19. For the three-block Gaussian model with mediator coupling ε, a pairwise representation of the reduced boundary exists exactly when $\varepsilon \geq 0.3333333$. Below the threshold the pairwise margin is $3\varepsilon - 1$, which is -0.4 at $\varepsilon = 0.2$; at the threshold it is 0 and the decomposition exists, is positive semidefinite, and reproduces the target.

The threshold is not an artefact of the parametrisation. Necessity is a trace inequality: each pairwise block must carry the off-diagonal entry $\pm\frac{1}{3}$ of the target, so a positive semidefinite block has diagonal sum at least $\frac{2}{3}$, and the three blocks together need at least two units of trace against the target's $1 + 3\varepsilon$. Sufficiency is an explicit decomposition, and at $\varepsilon = 0.3333333$ every block in it is rank one: the pairwise form sits on the boundary of the semidefinite cone there, and below it the cone is left. Two further disagreements belong with it. In Mueller's reduction control [Mueller, 2026, proposition 4], the two criteria disagree: the same observation scores 1, the first criterion scores 1 afterwards and the second -1, the response distance is 2, and the worst-case error has a lower bound of 1 — so the choice of criterion changes the verdict rather than the precision. And the iteration schedule is not a detail: the centred contrast after twelve steps differs between the full and the half-damped schedules by exactly 0.02304085 in absolute value, so a claim about "the" schedule path has to name the schedule [Mueller,

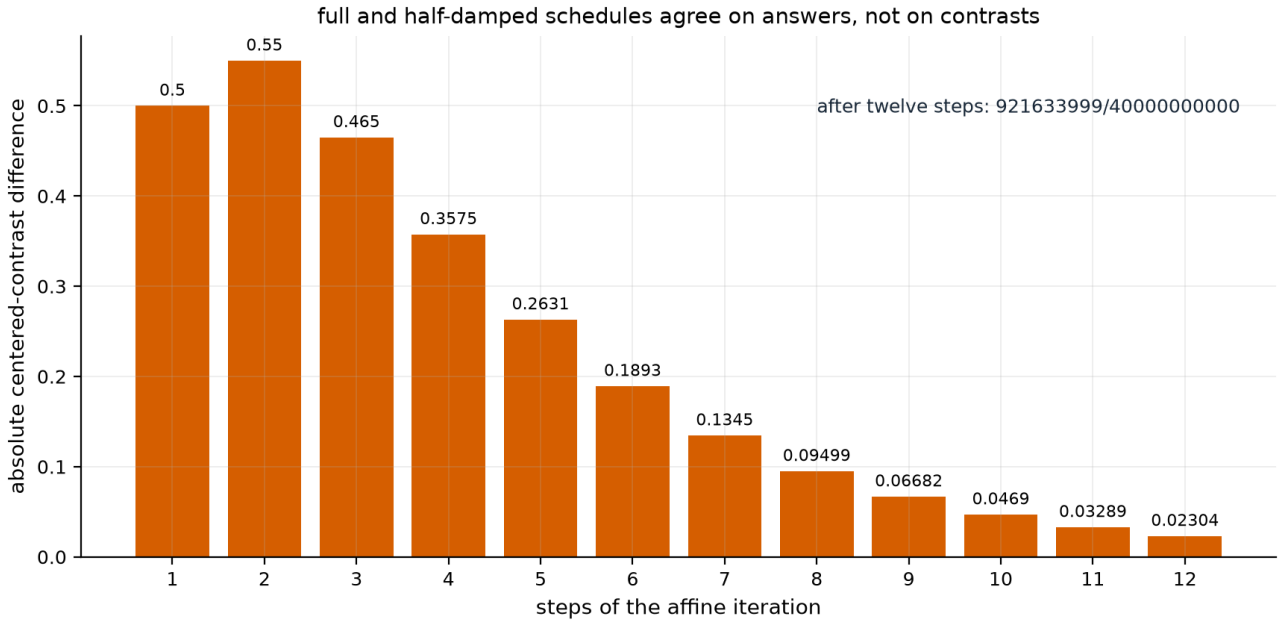


Figure 15: The absolute difference between the full and the half-damped schedules' centered contrasts, one exact value per step count from one to twelve. The schedules share every answer while the contrast difference decays to 0.02304085 after twelve steps: agreement and dissipation are state functions, and a finite schedule is not. Generated by `scripts/make_figures.py` from `core/controls.py`.

2026]. Registered as `mediator-obstruction`, with `reduction-criterion` and `schedule-path` beside it.

OPH's executable observer runs the reduction test on the native law itself [FloatingPragma, 2026, Mueller, 2026]. The source is uniform over the binary configurations. The observer repairs one seam, records the signed current, and chooses its second seam from that record alone. Over 264 equally weighted paths the final occupation of port zero is 35/264. With the selector disconnected, or driven by an independent record with the same seam frequency, it is 1/6, the occupation of the uniform binary state. The `reduction-criterion` probe enumerates the paths and checks the result against a case analysis that enumerates nothing. A summary that drops the record keeps the action frequencies and loses the response.

7.7 Existence does not imply reachability

The clipped map and the relaxation orbit reproduce Mueller's two-node control [Mueller, 2026, proposition 15].

Proposition 20. The two-node relaxation has Jacobian eigenvalues $1 \pm 2\,i$, a relaxation orbit whose radius stays in $[0.8400708,\ 1.053391]$ with period 7.575, and a synchronous clipped map whose orbit minimum radius is 1 — a different object with a different bound.

Mueller gives the bound 0.84 and period 7.58 [Mueller, 2026, proposition 15]. The probe measures 0.8400708 and 7.575. Both numbers are reported, because the difference between a source's bound and a package's measurement is exactly the kind of thing a reader needs to see rather than to trust. fig. 16 draws the orbit.

The disagreement is subtle and worth spelling out. Both programmes can prove that a fixed point exists, and both can compute it; the probe finds the complete fixed-point set of the clipped map by exact case analysis over its nine clipping regimes, and it is the origin alone. The synchronous orbit's radius bound is measured after a transient, which the probe records. The relaxation dynamics has a Jacobian with positive real part at the fixed point, so the fixed point is unstable, and the orbit is bounded away from it. Existence and reachability are different questions, and a synthesis that infers the second from the first is wrong in a way that no amount of algebraic care will fix. Registered as `existence-without-reachability`.

7.8 Direct and adjoint gradients differ

Mueller gives a two-dimensional example [Mueller, 2026, appendix B]. At its stable fixed point, with the non-symmetric Jacobian J and loss derivative c, a forward nudge measures the direct response $-J^{-1}c = (1, 0)$, while the gradient of the loss with respect to the parameters needs the adjoint $-J^{-\top}c = (1, 2)$, the recurrent back-propagation of [Pineda, 1987].

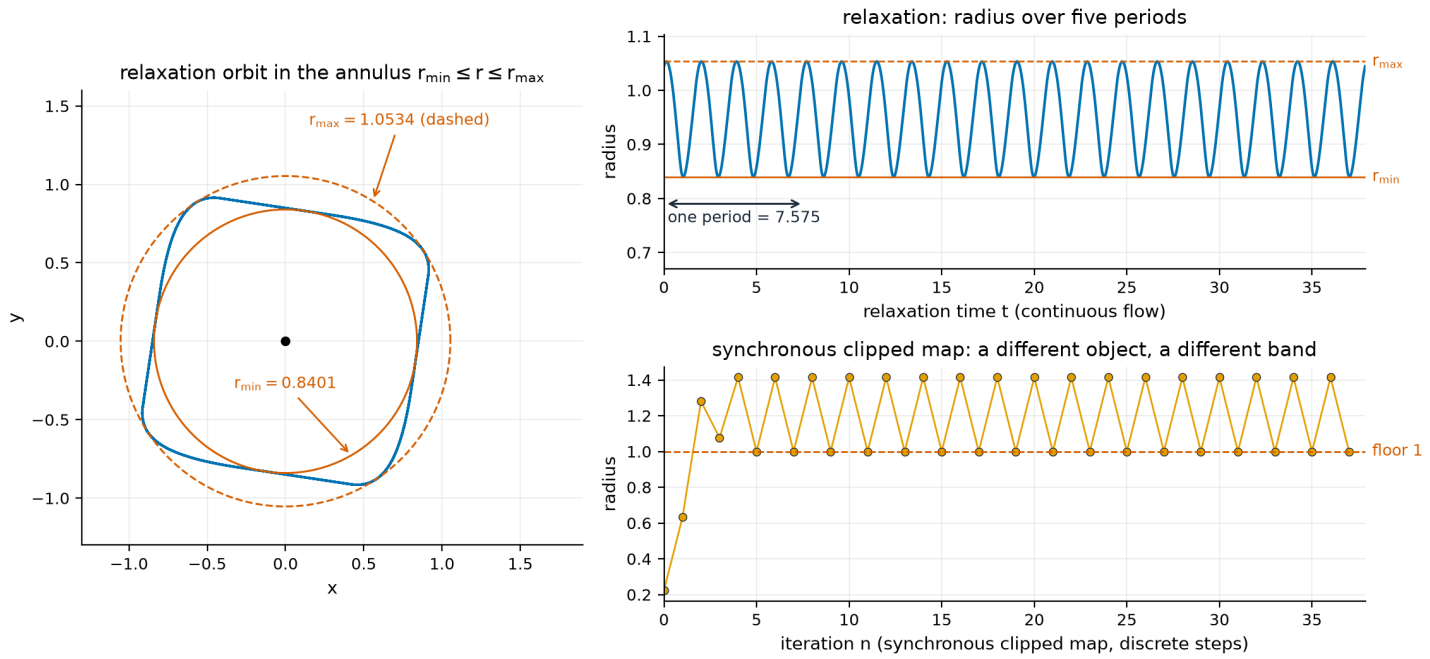


Figure 16: Existence without reachability. Left: the relaxation orbit in the plane, with the annulus $[0.8400708, 1.053391]$ that contains it; the orbit neither escapes nor reaches the origin. Right: the radius against time, showing the period 7.575 and the contrast with the synchronous clipped map, whose orbit is confined to a different annulus. Generated by `scripts/make_figures.py` from `core/controls.py::two_node_relaxation_orbit`.

Only the adjoint is the gradient; the two coincide exactly when J is symmetric, which is the case an energy-based network supplies. A learning rule that reads the forward response therefore does not follow the gradient of a directed network, and the disagreement is not a numerical artefact. Registered as `directed-gradient`.

7.9 The four-cycle has an incompatible local minimum

In Mueller's four-cycle control [Mueller, 2026, sec. 4.1], each edge carries an equality constraint. The compatible states are all-zeros and all-ones, with no violations, while the state `0011` violates two edges. Every single flip of that state also leaves two violations, so it is a (non-strict) *local* minimum of the violation count sitting on a plateau, and a descent method that only accepts strictly improving moves cannot leave it. The probe reports the violations after each of the four flips, all of which are 2.

This is the mechanism behind the traps that repair-as-descent arguments have to exclude by hand. It is also a concrete instance of the general point: a descent guarantee is a statement about a landscape, and a landscape with plateaux has local minima that are not global ones. Registered as `four-cycle-local-minimum`.

7.10 Twelve vertices is not one solid

The IVM's first shell and the carrier's vertex set both contain twelve points. That count is not an identification, and the probe exhibits the difference rather than the coincidence.

Proposition 21. The twelve nearest neighbours, joined when their squared distance is eight, form the cuboctahedron graph: 4-regular, 24 edges, eight triangles and six squares, with tetravolume 20. The carrier's graph is 5-regular with 30 edges and twenty triangles, and its solid has tetravolume 18.5123. The two graphs have the same vertex count and are not isomorphic.

The probe reports both degree sequences, both edge counts, both face decompositions, both volumes, and the fact that the icosahedral realisation of the carrier is isomorphic to the *carrier* and not to the neighbour graph. The tetravolumes settle it without reference to the graph at all: 20 against 18.5123..., one integral and one algebraic. The failure costs more than a footnote, because the two solids support opposite dynamical readings. The cuboctahedron's neighbours are arranged so that each vertex sees four others, which gives a lattice with a four-fold local order; the carrier's ports see five, which is what puts the surd $\sqrt{5}$ into the spectral gap $(5 - \sqrt{5})/60$ eq. 9 and what the FEP's blanket count of 5 inherits. A synthesis that identified the two by their common twelve would import a coordination number the carrier does not have.

Both solids are kissing arrangements of twelve spheres around one, which is where the confusion starts, and they attain the kissing number in different ways. With the twelve centres at twice the sphere radius from the centre, the cuboctahedron's squared edge over squared circumradius is 1, so every sphere touches four of its neighbours as well as the centre: the rigid arrangement of the densest packing. The icosahedron's ratio is $2-2\sqrt{5}/5 \approx 1.105573$, so its spheres touch the centre and none of each other. The slack is what Fuller's jitterbug uses to carry the vector equilibrium continuously through the icosahedron to the octahedron [Fuller and Applewhite, 1975, Verheyen, 1989], and the volume is not conserved along the way. Synergetics therefore does not conflate the two solids – it distinguishes them and connects them by a motion – and the obstruction is to a reader who identifies them by their count.

The same coincidence is why this entry is a disagreement rather than a complementarity: the neighbour *cell* of sec. 8.6 is the rhombic dodecahedron, of tetravolume six, whose twelve faces face the twelve neighbours and whose graph has six four-valent and eight three-valent vertices. Three distinct solids in this geometry have twelve-fold features, and only one of them is the carrier. Registered as `cuboctahedron-vs-icosahedron`.

7.11 The shell index and the free energy determine neither each other

Proposition 22. Let $F(z) = \frac{1}{2}\|z\|^2$ be the equal-covariance divergence of Proposition 11 at a lattice site z, and $k(z)$ its coordination-shell index (Definition 3). Neither is a function of the other. The first five shells carry (1, 3, 4, 7, 7) distinct values of F, and the levels (36, 52) are each carried by two shells. On shell k the divergence ranges from $2k^2$ (from $2k^2+2$ when k is odd) up to $4k^2$, and reaches $4k^2$ only at the twelve vertices $k\,m$.

The probe walks the shells, collects the distinct values of F on each, reports the counts per shell, the levels that appear on more than one shell, and the extreme values of F on every shell through 12. A shell is not a level set of F, and a level of F is not confined to one shell. The lower bound does give one inequality: $F \le L$ forces $k \le \sqrt{L/2}$, so a bounded free energy bounds the shell index from above. What fails is the identification, in both directions.

The reason is exact and easy to state once the shell has its closed form. The shell index is the gauge $g(u) = \max(\|u\|_\infty, \frac{1}{2}\|u\|_1)$ of eq. 8, a polyhedral norm whose unit ball is the vector equilibrium, while F is a Euclidean quadratic form whose level sets are spheres. A sphere and a cuboctahedron touch only along the cuboctahedron's twelve vertex directions, which is why F attains its shell maximum only at $k\,m$ and why the face points of shell k sit closer to the centre than its vertices, by up to a factor of $\sqrt{2}$ in distance.

fig. 17 draws both halves of the statement.

This is the paper's only *coordinate-level* obstruction. It does not say that the FEP's functional is wrong or that Synergetics' metric is wrong; it says that a composite vocabulary that treats "shell" and "free energy" as two names for the same stratification will be inconsistent at the first shell with more than one radius, which is shell two. Registered as `shell-vs-free-energy`.

7.12 The shells around a port are not the lattice's shells

Proposition 23. The ports at graph distance one, two and three from a port number (5, 5, 1), the graph is distance-regular with intersection array (5, 2, 1; 1, 2, 5) and diameter 3, and the lattice's own shells at the same three radii number (12, 42, 92).

The two sequences (5, 5, 1) and (12, 42, 92) disagree from the first term: the carrier's first shell is a port's 5 neighbours because the icosahedron is five-valent, while the IVM's first shell holds 12 sites because the lattice is twelve-coordinated by construction. The proposal that a port's neighbourhood is a lattice shell therefore fails on the smallest possible test, and no choice of radius repairs it: the carrier is finite with diameter 3, so its shells stop, while the lattice's do not.

What survives is a structural statement rather than an identification. The carrier is distance-regular, with intersection array (5, 2, 1; 1, 2, 5) read off a single representative per shell, so its neighbourhood structure is rigid: from any port, at any distance, the outward and backward degrees are the same [Brouwer et al., 1989]. That is a stronger fact than the identification it replaces, and it follows from the symmetry: the group of order 120 is transitive on the pairs of ports at each distance, and a distance-transitive graph is distance-regular.

7.13 `Twelve around one` names a family, not an object

Proposition 24. The phrase covers at least two solids with different counting invariants. The icosahedron is five-valent with 5184000 spanning trees; the cuboctahedron is four-valent, carries 8 triangles and 6 squares, 32 perfect matchings, and 331776 spanning trees, which is 576 squared.

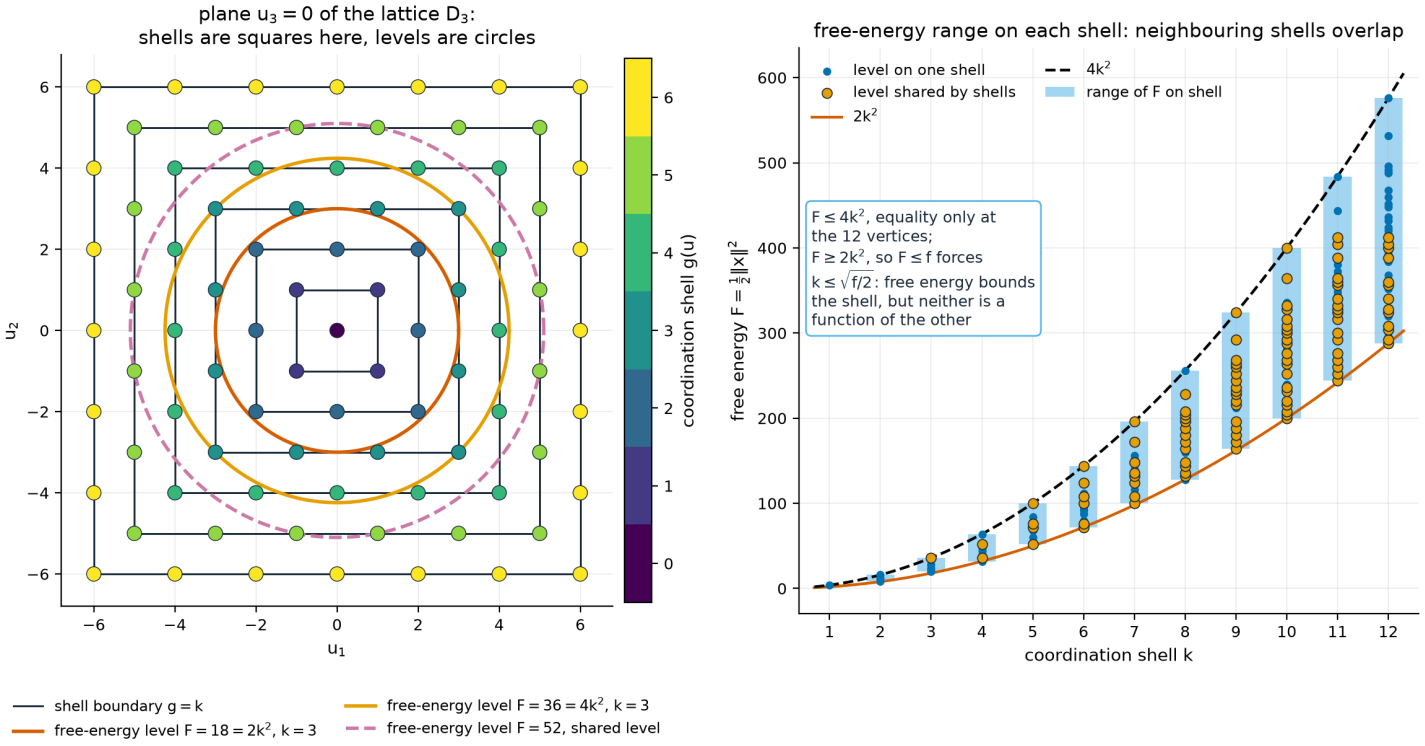


Figure 17: The coordination shell against the free energy. Left: the points of the face-centred cubic lattice D_3 in the plane $u_3 = 0$, coloured by the closed-form shell index g of eq. 8; in this slice the shells are nested squares, and the overlaid circles are levels of the free energy, which cross several shells. Right: for every shell through 12, the range of F over the shell as a bar and each distinct level as a dot, with the levels shared between shells highlighted and the curves $2k^2$ and $4k^2$ drawn; the maximum is attained only at the twelve vertices of each shell. A bounded free energy bounds the shell, and neither is a function of the other. Generated by `scripts/make_figures.py` from `geometry/lattice.py`.

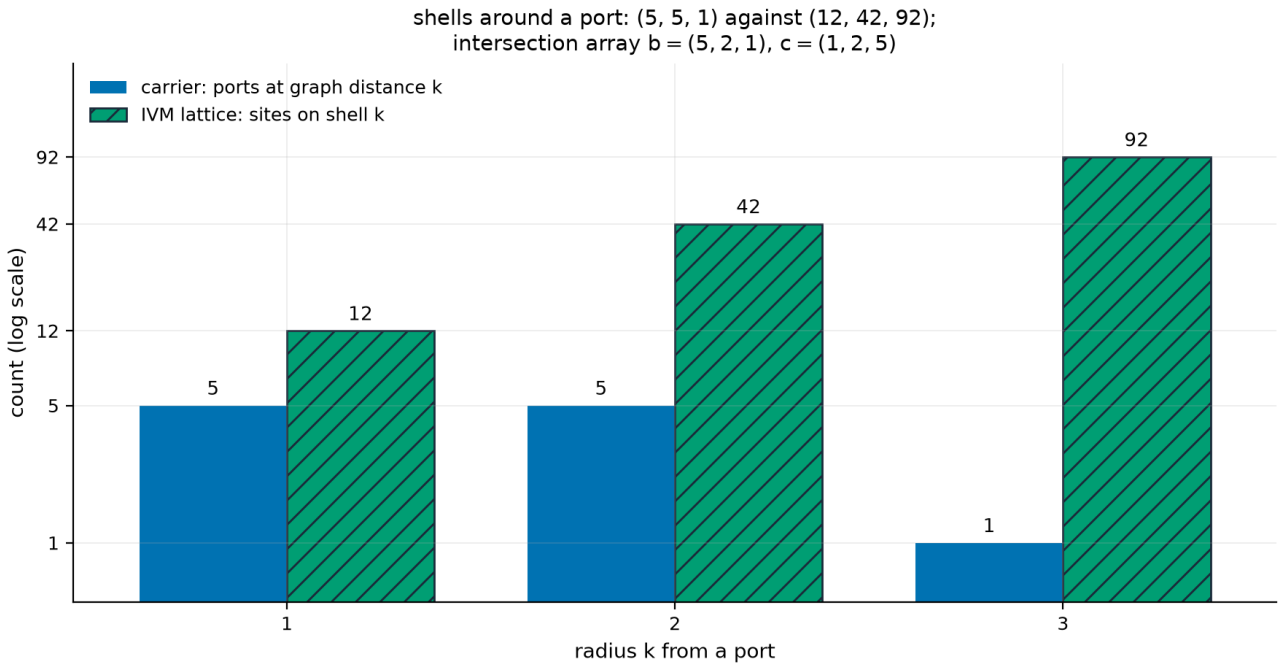


Figure 18: Two bar series against the radius from a port, on a logarithmic count axis. The carrier's ports number (5, 5, 1) at graph distances one, two and three, while the lattice's shells hold (12, 42, 92) sites at the same radii, so the sequences disagree at the first shell and no radius repairs the reading. The carrier is distance-regular, and the title annotates its intersection array (5, 2, 1; 1, 2, 5). Generated by `scripts/make_figures.py` from `core/network.py` and `geometry/lattice.py`.

This is the same failure sec. 7.10 reports, one level down. There the shared quantity was the vertex count; here it is the phrase itself. A reader who is told that a structure is "twelve around one" has been told the coordination number and nothing else, and the coordination number does not determine the object: the two solids differ in degree, in triangle count, in matching count, and in the spanning-tree number, whose ratio is exactly 125/8.

The counting invariant is what does the work. Spanning trees are computed by the same determinant (eq. 13; Proposition 8) in both cases, on adjacency matrices derived independently – the carrier's from OPH's oriented base faces, the cuboctahedron's from the neighbouring lattice sites – so the numbers are comparable even though the objects are not the same. What the registry records is that a claim of the form "the carrier is the twelve-around-one solid" is under-determined, and that the remedy is a refinement rather than a tolerance. Registered as `twelve-around-one-families`.

7.14 What the obstructions have in common

The obstructions fall into three kinds. The first is a *plateau*: zero-descent moves (PR-01), plateaux in the violation landscape (the four-cycle), and constant-energy swaps all describe dynamics that cannot be ordered into a descent. The second is a *missing invariant*: the entropy production of a stationary blanket, the stability of a coupling outside its stable region, and the direction of a gradient all vary within a class that a coarser vocabulary treats as fixed.

The third is the one a correspondence registry is best placed to catch: *an invariant too coarse to identify the object it is asked to identify*. Twelve vertices do not determine a solid (Proposition 21), the phrase "twelve around one" covers two solids it does not separate (Proposition 24), a port's neighbourhood is not a lattice shell (Proposition 23), and a shell index does not determine a free energy (Proposition 22). None of these failed because a number disagreed; each failed because the shared quantity was never an identification, and a table of matched counts would have reported each as a success.

A synthesis that wants to identify the three programmes must therefore add structure that excludes plateaux, fixes the missing invariants, and refines the coarse ones. That is a research programme, not a corollary, and the next section reports what each programme can contribute to it.

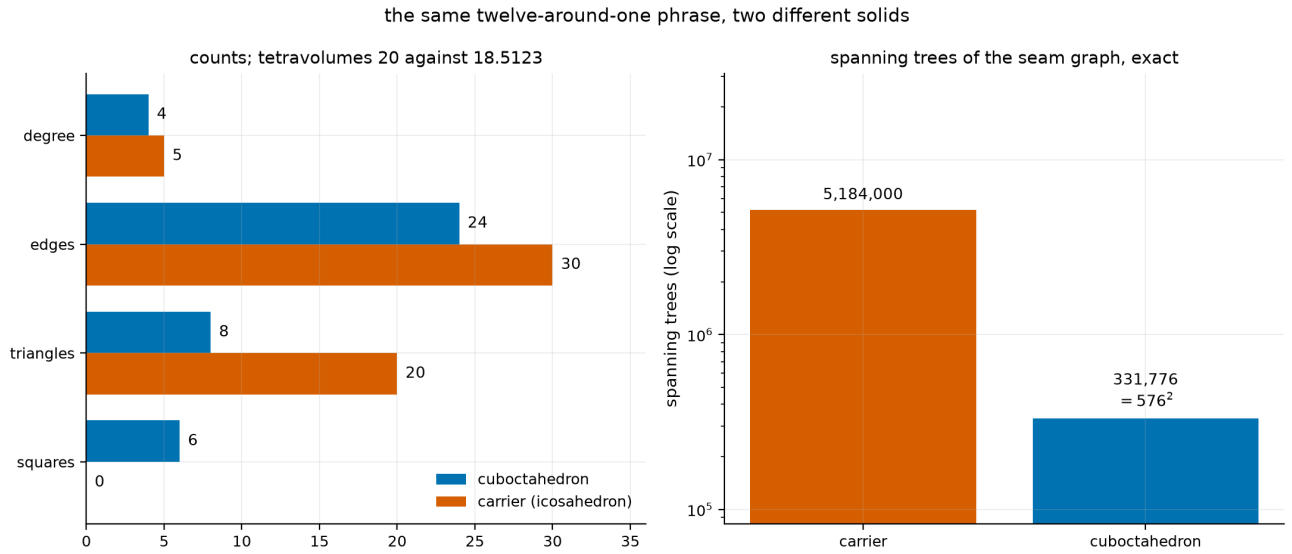


Figure 19: Two panels that separate the solids the phrase twelve-around-one can name. Left: the cuboctahedron's degree, edges, triangles and squares beside the carrier's — 4 against 5 neighbours, 8 triangles and 6 squares against twenty triangles and none, with the two tetravolumes annotated. Right: the spanning trees the same determinant counts — 5184000 for the carrier against 331776 for the cuboctahedron, which is 576 squared — on a logarithmic axis. Generated by `scripts/make_figures.py` from `core/invariants.py` and `geometry/lattice.py`.

8 Complementarity: structures one programme supplies and another needs

The 10 complementarities are not identifications and not failures. Each is a case where one programme supplies a structure that another needs and does not have, without either reducing to the other. They are the constructive part of the paper: most of them are geometric, the rest are a learning identity, a potential flow and a resistance metric, and two need all three vocabularies at once.

8.1 Synergetics supplies the accounting in which the carrier's geometry is exact

The carrier of Definition 1 is a graph. To draw it, to count its shells, and to state the volume of the polyhedra it bounds, a graph is not enough: a metric is needed, and the choice of metric decides which numbers come out exact. Synergetics supplies one in which they all do.

Proposition 25. The twelve quadray neighbour moves of eq. 7 are distinct, all have squared norm 8, and their minimum pairwise squared distance is also 8, so the twelve form a kissing configuration of radius $\sqrt{2}$. The coordination shells, enumerated, have `(1, 12, 42, 92, 162)` sites for $k = 0, \ldots, 4$ and cumulative counts `(1, 13, 55, 147, 309)`. The tetravolume table `tetrahedron 1, cube 3, octahedron 4, rhombic dodecahedron 6, cuboctahedron 20, truncated octahedron 96` is derived exactly: each solid is the convex hull of an explicit integer vertex set built from the lattice – the tetrahedron from the four axes, the cube from the axes and their negatives, the octahedron from the pairwise axis sums, the cuboctahedron from the twelve neighbours, the rhombic dodecahedron as their Voronoi cell, and the truncated octahedron by cutting the frequency-three octahedron at the thirds of its edges – and its volume, computed in rational arithmetic, is divided by the unit tetrahedron's.

The complementarity is exact and one-directional. OPH's dynamics does not need quadray coordinates, and the FEP does not need a lattice. But the moment the carrier is drawn, or its shells are counted as geometry rather than as graph distance, the quadray convention is what makes the statements exact rather than approximate. The derivation matters because a table is a claim: the cube's three and the truncated octahedron's ninety-six are conventions about *which* cube and *which* truncated octahedron (the cube whose face diagonals are the prime vector, and the truncated octahedron whose edge is), and only a vertex set fixes that choice. fig. 20 shows the shells and the volume ratios.

The kissing number is the point at which the two programmes touch. The carrier has 12 ports of degree 5; the IVM has 12 neighbours at squared distance 8; and the geometric icosahedron's adjacency is isomorphic to the derived carrier adjacency, which the probe checks by constructing a witness. The coincidence is not a numerological one: twelve is the kissing number in three dimensions [Schütte and van der Waerden, 1953, Conway and Sloane, 1999], and both arrangements

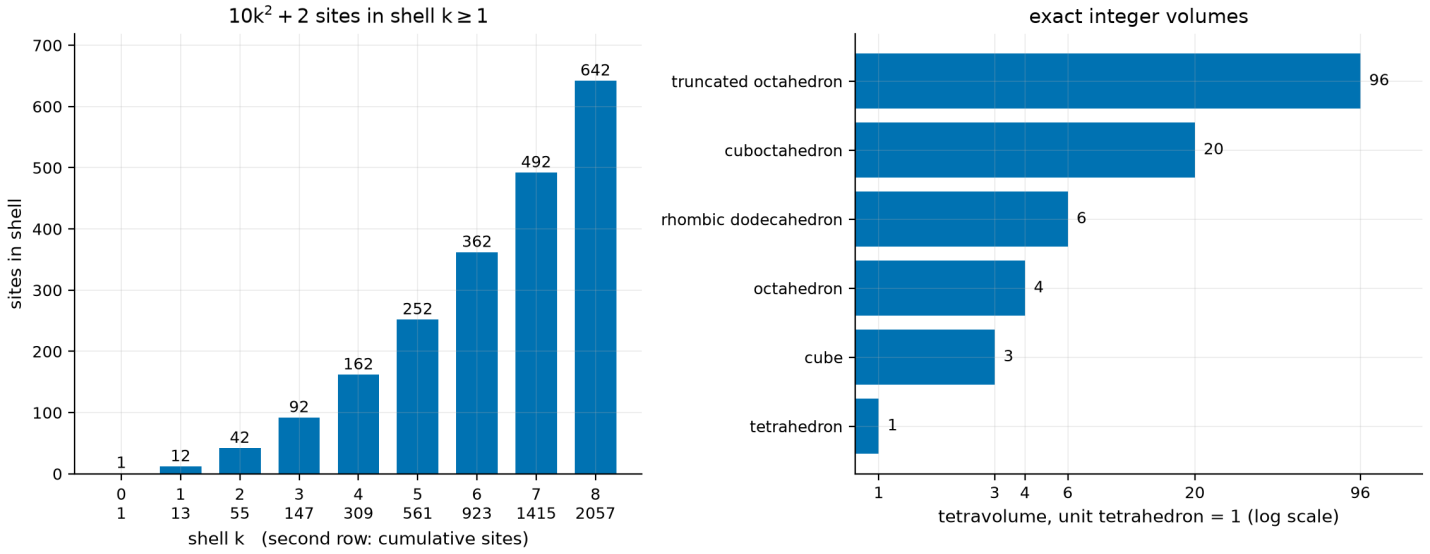


Figure 20: The IVM accounting. Left: shell sizes `10k^2 + 2` for $k = 0, \ldots, 8$ with the cumulative count overlaid; the first shell is the twelve-around-one configuration. Right: tetravolume ratios on a logarithmic scale, with the unit tetrahedron at one, so that the cube, octahedron, rhombic dodecahedron, cuboctahedron and truncated octahedron are all integers. Generated by `scripts/make_figures.py` from `geometry/lattice.py`.

attain it. They attain it differently, which the `kissing-twelve` probe measures exactly: the cuboctahedral arrangement is rigid, its spheres touching their neighbours, while the icosahedral one has slack, its squared edge over squared circumradius being $2 - 2\sqrt{5}/5 \approx 1.105573$ rather than 1 (sec. 7.10). The carrier is the loose arrangement; the lattice is the tight one.

8.2 The same quadratic sequence appears three times

Fuller's geodesic subdivision and Goldberg's dual construction produce the same pair of quadratic sequences, and the IVM shell count is one of them.

Proposition 26. For every frequency $f \geq 1$: the geodesic subdivision of the icosahedron has $10f^2 + 2$ vertices, $30f^2$ edges and $20f^2$ faces; its Goldberg dual has $20f^2$ vertices, $30f^2$ edges and $10f^2 + 2$ faces. Hence the vertex count of one is the face count of the other, and both are the IVM shell count of eq. 8.

This is the clearest complementarity in the paper, and the least mysterious. Duality swaps vertices and faces, so the two counts trade places, and Euler's formula with twelve five-valent vertices fixes the rest. The IVM shell count is the same quadratic for a combinatorial reason: the frequency-f shell of the vector equilibrium has eight triangular and six square faces of frequency f, and cutting each square along a diagonal turns it into the frequency-f geodesic icosahedron on the same vertex set, which is the move Fuller's jitterbug makes continuously [Fuller and Applewhite, 1975, Verheyen, 1989]. The geodesic counts are the $T = f^2$ case of the Caspar-Klug classification of icosahedral shells [Caspar and Klug, 1962, Coxeter, 1973]. What Synergetics adds is the insistence that the *volume* accounting is exact in the same convention, which is what makes the subdivision usable as a discretisation rather than only as a drawing.

8.3 Energy-based learning supplies the gradient the repair law lacks

Equilibrium propagation is the cleanest case in which an energy is not merely a bound but a computational device: perturb the output, let the system relax, and read the gradient from the difference in the relaxed energy [Scellier and Bengio, 2017]. It belongs to energy-based learning rather than to the FEP, which reaches the same territory through predictive coding: inference by settling a precision-weighted prediction-error energy approximates back-propagation [Whittington and Bogacz, 2017, Millidge et al., 2022]. The probe is a scalar energy model, chosen so that every quantity has a closed form.

Proposition 27. At perturbation β, the closed-form contrast is -1.2499987500012502 and the relaxed contrast is -1.24999874998033, against an exact gradient of -1.25. The closed-form error is 2.092015e-11 and the distance to the gradient is 1.249999e-06, matching the predicted $O(\beta)$ scaling.

The complementarity is that an energy provides the *objective* and the relaxation dynamics provides the *implementation*, and

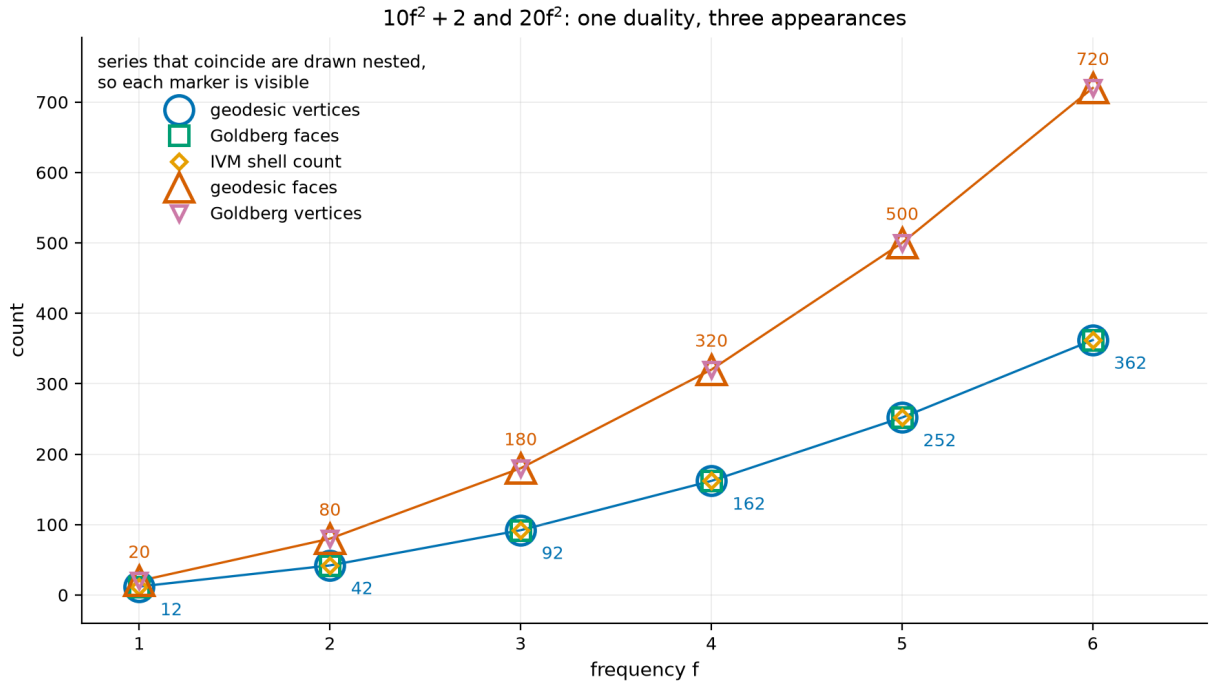


Figure 21: Three appearances of one sequence. The geodesic vertex count `10f^2 + 2`, the Goldberg face count, and the IVM shell count are the same function of the frequency, while the geodesic face count and the Goldberg vertex count are `20f^2`. The plot shows both sequences against f and annotates the duality. Generated by `scripts/make_figures.py` from `geometry/subdivision.py`.

the identity between them is exact to the stated order in the perturbation. It needs a symmetric interaction, which is why the directed case of sec. 7.8 is an obstruction. Neither OPH's repair rule nor Synergetics' accounting gives such an identity, and neither needs one.

8.4 Selection supplies a potential flow, for symmetric payoffs

Proposition 28. For a symmetric payoff A, the replicator field $\dot{x}_i = x_i((Ax)_i - x^\top Ax)$ equals $M(x)\nabla F$ with $F = \frac{1}{2}x^\top Ax$ and mobility $M = \mathrm{diag}(x) - xx^\top$, at every point checked, with the direct potential rate 0.1344 agreeing with the rate computed through the mobility and the field norm 0.2119623 at the reported point. For a non-symmetric payoff the same identity fails at every point checked.

The replicator equation for a symmetric (partnership) game is a gradient flow in the Shahshahani metric [Shahshahani, 1979, Taylor and Jonker, 1978, Hofbauer and Sigmund, 1998], and the mean payoff is a Lyapunov function for it. The probe checks the identity, not merely the sign, and checks its boundary: with an asymmetric payoff the field is still $M(x)Ax$, but no potential reproduces it.

The relevance to the three programmes runs through inference. The discrete replicator equation is Bayes' rule, with types as hypotheses and fitness as likelihood [Harper, 2009], so the FEP's posterior updating and selection share one dynamical form, and this is the one place where a potential is unambiguously a Lyapunov function of a dynamics that appears in population biology rather than in neuroscience. It supplies a template: a synthesis that wants a free-energy descent for OPH's repairs should look for the metric in which the repair field is a gradient, and the replicator case shows what such a metric looks like when it exists. Registered as `replicator-potential`.

8.5 The carrier's own solid has an exact algebraic volume

The tetravolume table of sec. 8.1 is a table of integers, and the carrier's own solid is not in it. It has an exact volume all the same, and the fact that the volume is exact while being algebraic rather than integral is the sharpest statement of what the synergetic convention buys.

Proposition 29. The regular icosahedron whose edge is the prime vector has tetravolume 18.5123, equal to $\frac{5}{2}(3\sqrt{2}+\sqrt{10})$ exactly, and the square of that tetravolume is 342.7051, which is exactly $175+75\sqrt{5}$. Its twelve vertices are 5-valent, and its

twenty triangles are all congruent.

The probe computes the volume twice. The exact route places the icosahedron of edge two at $(0, \pm 1, \pm\varphi)$ and its cyclic permutations, with $\varphi = (1+\sqrt{5})/2$, finds its twenty facets by an exact supporting-plane test, and sums signed tetrahedra in the field $\mathbb{Q}(\sqrt{5})$; dividing by the regular tetrahedron of the same edge gives the tetravolume as $\sqrt{2}$ times `15/2 + 5/2 sqrt 5` exactly, with no rounding anywhere. The floating-point route applies the divergence theorem to the measured surface and divides by the same tetrahedron, and the two agree to the last digit, so the agreement is an identity rather than a tolerance chosen to make it hold.

Two details of the computation are worth recording because they are corrections rather than conveniences. The first is that a face list is an *unordered* set of triangles: ten of the twenty faces enumerated from the vertex set come out facing inward (10 of them), and the signed sum cancels exactly before they are reoriented. The second is that the tetravolume convention is a convention: changing the unit tetrahedron rescales every entry in the table, and the claim made here is the ratio the convention defines and not an absolute volume.

Why this is a complementarity rather than an identification is now visible. OPH supplies the graph, and the graph's faces are triangles; Synergetics supplies the convention in which those triangles have exactly computable volumes; and neither programme as written states the volume of the solid its own graph bounds. The table's integral entries and the carrier's algebraic entry belong to the same accounting, which is what makes the disagreement of sec. 7.10 a statement about solids and not about conventions.

8.6 The densest packing in three dimensions has the twelve-around-one cell

Proposition 30. The Voronoi cell of the twelve neighbours has 14 vertices, 12 rhombic faces and 24 edges, with Euler characteristic two and no orientation flips. Its tetravolume is 6, and the ball of radius half the prime vector inscribed in it has tetravolume 4.442883, so the packing fraction is 0.7404805, equal to $\pi/(3\sqrt{2})$.

This is the paper's clearest case of a number that can be *derived* instead of read. The tetravolume of the cell is computed from the halved squared norm at each of its fourteen vertices, using the same quadratic form that makes the neighbour distances exact, and it arrives at six: the same six the synergetic table lists for the rhombic dodecahedron. A reader who suspects that a table entry is a stylised fact can therefore check it by an independent route, which is the pattern this package uses wherever a source table has consequences.

The density is then derived rather than quoted, and it is exact. The cell has integer vertices, so its volume is computed in rational arithmetic and its tetravolume is exactly 6; the inscribed ball has radius $\sqrt{2}$, half the prime vector, so its tetravolume is exactly $\pi\sqrt{2}$; and the density is their ratio, $\pi\sqrt{2}/6 = \pi/(3\sqrt{2}) = 0.7404805$. That number is the Kepler density of the face-centred cubic arrangement, of which the IVM's twelve neighbours are the local picture. It is optimal among lattice packings [Gauss, 1840] and among all packings [Hales, 2005, Hales et al., 2017]. The complementarity is that Synergetics' twelve-around-one is not a drawing convention but the local configuration of the densest packing in three dimensions.

The carrier does not inherit that optimality, and the same cell is the reason the disagreement of sec. 7.10 is not a quibble. The densest packing's kissing arrangement is the rigid cuboctahedral one, whose cell is the rhombic dodecahedron of tetravolume six; the carrier's solid is the loose icosahedral arrangement, of tetravolume 18.5123, with a 5-regular graph. Both put twelve spheres around one, and they are different objects.

8.7 Three number systems and no common unit

Proposition 31. The three programmes' exact quantities live in different number systems. The FEP's divergence for one IVM step is the integer 4 nats (with unit covariance in the default embedding); the carrier's normalised spectral gap, a relaxation rate of OPH's mean repair operator, is the quadratic surd $(5-\sqrt{5})/60 \approx 0.04606553$; and Synergetics' table is integral, with the twelve-neighbour cell at 6, while the carrier's own solid lies in $\sqrt{2}\,\mathbb{Q}(\sqrt{5})$.

This is one of the two entries in the registry that need all three vocabularies at once – the other is the conjugation norm of sec. 8.10 – and both are complementarities rather than identifications for that reason. The three quantities are attached to different objects (a mean shift, a relaxation, a solid), so none is the "cost of a step" in another's terms, and no common unit converts one into another: an integer, a surd and an element of a biquadratic field cannot be made equal by rescaling. A reader who wants one number has to choose a currency and state the exchange rate; a reader who wants the object has three exact readings of it.

8.8 The precision also carries a resistance metric

Proposition 32. Ground the Laplacian at one port and solve $Lx = e_i - e_j$ over the rationals [Klein and Randić, 1993]: the effective resistance across a seam is 11/30, at distance two 7/15, and across the carrier 1/2, over (30, 30, 6) pairs in the three classes, summing to a Kirchhoff index of 28.

In the Gaussian reading, this resistance is the variance of the intrinsic potential difference. The probe `two-record-resistance` eliminates all free ports and compares the resulting pairwise Schur complement with the grounded network solve for every pair. For records o_i, o_j, the Schur term in eq. 4 is $(o_i - o_j)^2/(2R_{ij})$. The proper prior then contributes its own energy and the record normaliser.

Across the carrier, the three classes contribute 28 in total, and the same total is twelve times the reciprocal spectrum sum 7/3 from sec. 6.9, which is a cross-check between a rational system solved pair by pair and a closed-form spectral identity. The agreement is exact and the two routes share no arithmetic. Registered as `effective-resistance`.

8.9 The twelve-around-one cell and the cuboctahedron are duals

Proposition 33. The cell of the twelve neighbours and the cuboctahedron are dual edge for edge: 14 vertices against 12, 12 faces against 14, and 24 edges each, with Euler characteristic two each and tetravolumes 6 and 20, the cuboctahedron's to the cell's in the ratio 10/3.

The dual pair is derived twice, and the two derivations meet. The cell is built from the constraints of the twelve lattice sites, and the cuboctahedron from the neighbouring sites themselves; the cuboctahedron is also the cube's line graph, which the probe asserts by an explicit isomorphism search over the twelve vertices rather than by comparing degrees. sec. 8.6 uses the cell for a density; this claim records that its partner is the other solid Synergetics names for the same arrangement, and that the two accountings are related by exactly 10/3.

8.10 Conjugation fixes the counts and moves the volumes

Proposition 34. Conjugating $\sqrt{5}$ while fixing $\sqrt{2}$ leaves the counting invariants alone and moves the geometric ones. The spanning-tree number 5184000 is a rational integer and is fixed; the icosahedron's tetravolume 18.5123, $\sqrt{2}$ times `15/2 + 5/2 sqrt 5`, maps to 2.700908, and the two multiply to exactly 50, computed in field arithmetic.

This is the sharpest statement the paper can make about the difference between its two kinds of claim, and it is why sec. 9 separates them. A count over a finite complex is an integer, so the Galois symmetry of the quadratic field cannot see it; a volume in the same field is not an integer, and the symmetry moves it to a value that no solid of the table has. The product of the two is an integer, 50, so the conjugation is a check rather than a curiosity: a transcription error in either volume would break a product that is exactly rational. Registered as `conjugation-norm`.

8.11 What the complements add up to

The 10 complements partition the labour cleanly. Synergetics supplies a metric, a volume convention and an exact packing in which the carrier's geometry is computable rather than merely drawable. The FEP supplies a functional and a bound, and, through predictive coding and the replicator's reading as inference, reaches two identities – the energy-based learning gradient and the Shahshahani potential flow – that make the functional computationally and dynamically meaningful. OPH supplies a finite substrate and an explicit local update that neither of the others has.

Each complement is stated as a numbered proposition: the quadray accounting (Proposition 25), the subdivision identity (Proposition 26), the learning identity (Proposition 27), the replicator metric (Proposition 28), the carrier's solid (Proposition 29), the packing (Proposition 30), the three number systems (Proposition 31), the resistance metric (Proposition 32), the dual pair (Proposition 33) and the conjugation check (Proposition 34).

The synthesis that the complements suggest is therefore not a reduction but an assignment: the carrier is OPH's, the functional is the FEP's, and the accounting is Synergetics'. Two of the complements add a reading neither programme asks for and both can use: the precision's own resistance metric, and the conjugation that separates the counts from the volumes. sec. 9 states the limits of that assignment.

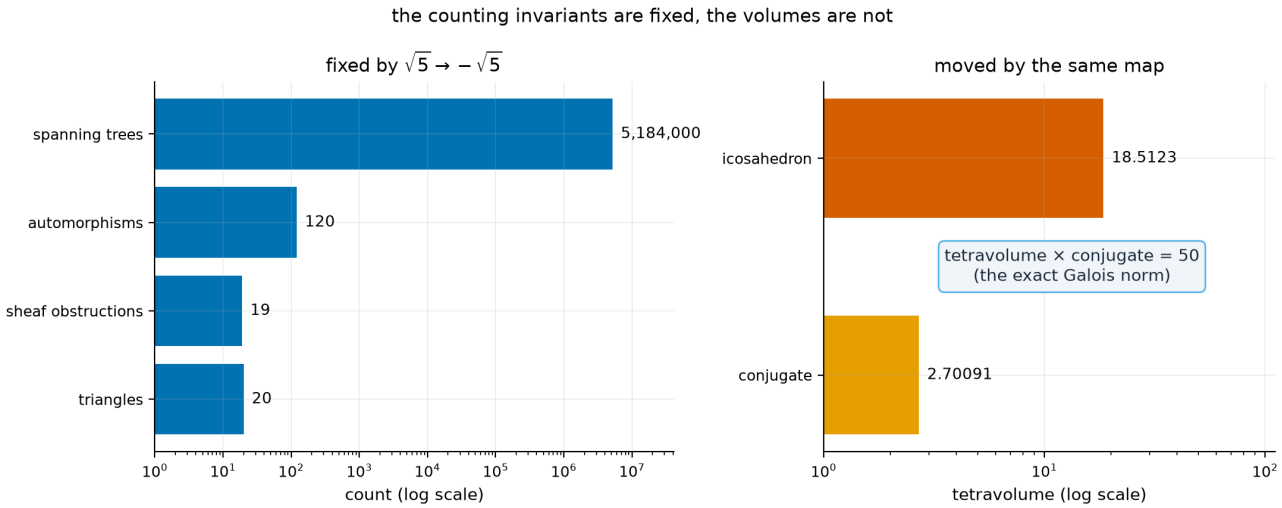


Figure 22: Two panels on logarithmic axes. Left: the counting invariants that conjugating the square root of five fixes: the spanning-tree number 5184000, the automorphism group order 120, the 19 sheaf obstructions and the 20 triangles. Right: the icosahedron's tetravolume 18.5123 beside its conjugate 2.700908; the two multiply to the exact norm 50. Generated by `scripts/make_figures.py` from `geometry/solids.py` and the bound values.

9 Scope, limits and falsifiers of a correspondence battery

9.1 What is verified

Everything in sec. 6, sec. 7 and sec. 8 is executed by `oph-fep-synergetics verify`, which runs 44 probes and exits non-zero if any of them fails. The command can be narrowed to one pairwise scope with `--pair`, so a reader who only wants the Synergetics–OPH ledger does not have to take the rest on trust. The values quoted in the prose are the values the probes report; a change in any of them changes the probe's output and, where the change is a failure, changes the exit code.

Four limits of that verification should be stated.

The first is domain. The variational equivalence Proposition 5, the dictionary sec. 6.6 and the two FEP identities hold in the linear-Gaussian corner. The results are exact there and are not claimed elsewhere. Where a probe can test the boundary of the domain — the `exact-on-domain` entries — it does, and the status vocabulary records the difference.

The second is size. The carrier has twelve ports, and the shell census is exhaustive over a set of 78 configurations. Both are small enough to enumerate and too small to settle any question about scaling. Nothing in this paper claims that the identities survive a continuum limit, and the obstruction results in particular are statements about this carrier.

The third is provenance. The source for the dynamical controls is a preprint [Mueller, 2026], and OPH's own results are stated in its synthesis paper [Mueller et al., 2026]. The preprint's propositions are cited as the source states them, the package's own measurements are reported alongside, and a reader who disagrees with the preprint can still use the measurements. The three software programmes are pinned to commits, and the pins are point-in-time readings rather than perpetual guarantees.

The fourth is arithmetic. The counting identities are exact: the spanning-tree number is an integer determinant computed over the rationals, the cohomology dimensions are exact ranks, the reciprocal spectrum sum comes from an exact rational inverse, the group order and its rotation/reflection split are integers, and the equivariance claim is a finite search over 120 group elements and 78 configurations. The geometric claims are exact too wherever the geometry allows: the tetravolume table, the cell's volume and the icosahedron's tetravolume are computed in the rationals and in $\mathbb{Q}(\sqrt{5})$ from exact vertex sets, and the floating-point measurements are reported beside them as a second route. What stays floating-point is what has to: the eigenvalue locus, the relaxation orbit and the free-energy values of the linear-Gaussian model, whose probes report residuals and use tolerances stated in the code. The cleanest statement of the two kinds of claim is the conjugation of $\sqrt{5}$, which sec. 8.10 turns into a probe: it fixes the integer counts and moves the volume to 2.700908, and the two volumes multiply to exactly 50. A counting claim in this paper is therefore invariant under a symmetry that a geometric claim is not, and comparing one against the other without saying so is the error the section is written to prevent.

9.2 Three source quantities and their protocols

The source states three numbers for the native law [Mueller, 2026]. Each is determined by a protocol in OPH's public model [FloatingPragma, 2026], and the registry reproduces all three exactly (tbl. 6).

Table 6: The source quantities and the protocols that determine them. sec. 7.1 and sec. 7.6 report the values with their controls.

Quantity	Protocol	Probe
13/15 and 1/60	one attempt, a uniform seam and a fair coin, from the configuration with one unit on each of two adjacent ports: staying put, and one particular hop	`pr01-obstruction`
35/264	uniform binary source, two repair events, the second seam chosen from the first recorded current: the mean final load at port zero	`reduction-criterion`

The status `not-reproduced` stays in the vocabulary for a quantity whose protocol no source states. No entry of the registry carries it.

9.3 What is not claimed

This paper does not claim that Observer Patch Holography is a free energy principle. It does not claim that the Free Energy Principle is a holographic theory. It does not claim that Synergetics predicts either. It does not claim that any of the three is empirically adequate; OPH's own empirical status document is explicit that no retained laboratory comparison selects a native record law, and this paper inherits that position rather than improving on it [FloatingPragma, 2026].

It also does not claim novelty for the mathematics. The spectral theory of cellular sheaves, the Routh criterion, the Markov-blanket critique, and the Goldberg construction are all prior work; what is new here is the *conjunction* of them on one finite object, and the discipline of reporting which conjunctions fail.

9.4 Four cautions for anyone continuing this work

The source dossier states four cautions, and this paper adopts them [Friedman, 2026a].

Disambiguate "free energy". At fixed records, name the minimum interface energy, the unnormalised record potential, or the normalised record surprisal that bounds variational free energy sec. 7.2.

Respect premise discipline. OPH's PR-01 describes the native implementation and distinguishes it from the contracts with consensus theorems. The native and gated relations have different obstructions Proposition 15; a conclusion about one is not a certificate for the other.

Distinguish numerology from prediction. The twelve-fold and sixty-fold coincidences in this paper are derived, and the derivation is part of the probe. A numerical coincidence that is not derived is not evidence, and the Synergetics literature contains both kinds. The counting obstructions are the sharpest examples: twelve-fold features are shared by a cuboctahedron, a rhombic dodecahedron (twelve faces) and an icosahedron, and only one of the three is the carrier sec. 7.10.

Respect scale separation. The linear-Gaussian results are exact at finite size and say nothing about a continuum limit. A claim that survives at twelve ports may fail at a thousand, and the paper's obstruction results are the ones most likely to change with scale.

9.5 What would change the conclusions

The conclusions are falsifiable in a specific sense, and it is worth saying how.

A single strict descent at $|d| = 1$ would disprove Proposition 14 and remove the PR-01 obstruction. A pairwise representation below $\varepsilon = 0.3333333$ would disprove Proposition 19. A member of the solenoidal family with a different entropy production would disprove Proposition 17. A stable $D_k A$ at $k > \sqrt{10}$ would disprove Proposition 18. A lattice site whose breadth-first shell differs from its cuboctahedral gauge would disprove Definition 3, and a transition that fails to commute with an automorphism would disprove Proposition 10. Each of these is a computation, not an interpretation, and each is executable against the package as it stands.

That is the property this paper was built for: the disagreements are as checkable as the agreements, and either can be overturned by running a function.

10 Reproducibility: pins, commands, and the binding of every number to a function

10.1 What this manuscript is made of

The manuscript is a project of the `docxology/template` research monorepo: LaTeX is produced by Pandoc, citations are resolved with `--natbib` against `references.bib`, equations are numbered by `pandoc-crossref`, and formal statements are numbered by the repository's `formalism.lua` filter, so that a definition or a proposition has the same number in every rendered edition [Friedman, 2026d].

Every number in the prose is a brace-delimited token resolved at build time from `manuscript_variables/values.py`, which binds each value to the function or source that produces it. A token that the generator does not emit fails the build, and a value that changes changes the prose. The binding is the reason the paper can claim that its numbers are not transcribed.

Table 7: Which surfaces are written by hand and which are produced. A generated surface is never edited to make a check pass; the producer is changed instead.

Surface	Authored	Generated
`manuscript/*.md`	yes	never
`references.bib`	yes	never
`src/`, `geometry/`, `analysis/`	yes	never
`../figures/*.png`	no	`scripts/make_figures.py`
`../figures/figure_registry.json`	no	`scripts/make_figures.py`
`docs/CORRESPONDENCES.md`, `docs/MANUSCRIPT_VALUES.md`, `docs/CONCORDANCE.md`	no	`scripts/render_docs.py`
manuscript tokens	no	`scripts/z_generate_manuscript_variables.py`

10.2 The three source pins

The three programmes are read at pinned commits. The commit itself lives in `data/sources.json` and is reported by `oph-fep-synergetics sources`, which also reports whether the live checkout still matches it.

Table 8: The three pins. The `Recorded` column is the number of identifiers the pin file attributes to each source; each identifier names a file, a line range and a symbol, so that a reader can check the reading rather than trust it.

Source	Repository	Licence	Recorded
Observer Patch Holography	`FloatingPragma/observer-patch-holography`	Apache-2.0 (software) and CC BY-NC-SA 4.0 (papers, data, ledgers)	commit, branch, thirteen cited identifiers
FEP_Formal	`ActiveInferenceInstitute/fep_formal`	CC BY 4.0, DOI `10.5281/zenodo.19699233`	commit, branch, four cited identifiers
QuadMath	`docxology/QuadMath`	Apache-2.0, DOI `10.5281/zenodo.16887791`	commit, branch, five cited identifiers

A pin is a reading, not a promise. `oph-fep-synergetics sources` reports `match` when the live checkout is at the pinned commit, `moved` when it has advanced, `absent` when the checkout is not present, and `unavailable` when Git cannot be queried. A `moved` result is not a failure: it says the reading is historical.

10.3 The commands

```
# the suite, and the coverage gate (90% branch minimum)
.venv/bin/python -m pytest tests/ --cov --cov-report=term-missing
```

```
# every correspondence, in one run or one pairwise scope at a time
.venv/bin/oph-fep-synergetics verify
.venv/bin/oph-fep-synergetics verify --pair synergetics-oph
.venv/bin/oph-fep-synergetics verify --kind disagreement
.venv/bin/oph-fep-synergetics verify --json

# the pins, checked against the live checkouts
.venv/bin/oph-fep-synergetics sources --vault-root /path/to/vault

# the figures and their accessibility registry
.venv/bin/python scripts/make_figures.py

# the generated reference documents
.venv/bin/python scripts/render_docs.py --check

# the manuscript tokens, then the PDF; both run from the template checkout
cd /path/to/template
TEMPLATE_REPO_ROOT=$PWD .venv/bin/python /path/to/project/scripts/z_generate_manuscript_variables.py
.venv/bin/python scripts/pipeline/stage_03_render.py --project working/OPH-FEP-Synergetics --skip-manuscript-h
```

: The reproduction commands, in order. The plain `verify` runs all 44 probes; `--pair` runs one ledger, of 26, 14, 2 and 2 claims respectively, and `--json` writes the same report as machine-readable values. The last two commands run from the `docxology/template` checkout, because the rendering infrastructure lives there. {#tbl:commands}

10.4 Environment

The package depends on `numpy` and on nothing else at run time; the test and figure extras add `pytest`, `pytest-cov` and `matplotlib`. The supported interpreters and library versions are the lower bounds in `pyproject.toml` (`CPython >= 3.12`, `numpy >= 1.24`), and `scripts/build.py` prints the interpreter and numpy versions of the run that produced a given PDF. Every exact value – the counts, the ranks, the tetravolume table, the icosahedron's volume in $\mathbb{Q}(\sqrt{5})$ – is computed in Python's `fractions` arithmetic and does not depend on the numpy version. The suite has no network dependency; the provenance check reads the local checkouts with `git rev-parse` and reports `absent` when they are not mounted.

The rendering toolchain is `Pandoc 3.13` with `pandoc-crossref` and a TeX Live installation. The template's own documentation records the full toolchain [Friedman, 2026d]; this section records only what the manuscript needs.

10.5 What a reader should check first

A reader who wants to test the paper rather than read it should run three commands. `oph-fep-synergetics verify` reproduces every number in sec. 6, sec. 7 and sec. 8 and exits non-zero on any failure. `oph-fep-synergetics sources` shows whether the three readings are still current. And `pytest` shows whether the values the prose quotes are still the values the code returns, which is the property that makes this paper different from a summary of three literatures.

11 References

The bibliography is `references.bib`, read by Pandoc during the PDF render. The build invokes Pandoc with `--natbib`, so every `[@key]` citation in the manuscript is rewritten to the corresponding LaTeX command and resolved against the bib file.

Three entries are provenance records rather than literature: `oph`, `fepformal` and `quadmath` identify the pinned checkouts, their licences and their DOIs. A reader who wants the exact commits should read `data/sources.json` or run `oph-fep-synergetics sources`, which reports the live status of each pin rather than repeating a snapshot here.

The bibliography is validated for syntax and for the required fields of each entry type by the template's citation validator:

```
uv run python -m infrastructure.reference.citation.cli validate \
    projects/working/OPH-FEP-Synergetics/manuscript/references.bib --strict
```

The validator path above is template-internal: it resolves inside the `docxology/template` monorepo and does not exist in this repository, where the equivalent public check is the repository's own render contract, `scripts/check_render.py`. The pre-digital books are cited the way they can be verified: *Synergetics* by publisher and year, while the full text of its second volume is archived, with the address carried in the bibliography.

Miguel Aguilera, Beren Millidge, Alexander Tschantz, and Christopher L. Buckley. How particular is the physics of the free energy principle? *Physics of Life Reviews*, 40:24–50, 2022. doi: 10.1016/j.plrev.2021.11.001.

Shun-ichi Amari. *Information Geometry and Its Applications*. Springer, Tokyo, 2016. doi: 10.1007/978-4-431-55978-8.

Ping Ao. Potential in stochastic differential equations: novel construction. *Journal of Physics A: Mathematical and General*, 37(3):L25–L30, 2004. doi: 10.1088/0305-4470/37/3/L01.

Kenneth J. Arrow and Maurice McManus. A note on dynamic stability. *Econometrica*, 26(3):448–454, 1958. doi: 10.2307/1907624.

Martin Biehl, Felix A. Pollock, and Ryota Kanai. A technical critique of some parts of the free energy principle. *Entropy*, 23 (3):293, 2021. doi: 10.3390/e23030293.

Andries E. Brouwer, Arjeh M. Cohen, and Arnold Neumaier. *Distance-Regular Graphs*. Ergebnisse der Mathematik und ihrer Grenzgebiete (3). Springer, Berlin, 1989. doi: 10.1007/978-3-642-74341-2.

Jelle Bruineberg, Krzysztof Dołęga, Joe Dewhurst, and Manuel Baltieri. The emperor's new markov blankets. *Behavioral and Brain Sciences*, 45:e183, 2022. doi: 10.1017/S0140525X21002351.

D. L. D. Caspar and A. Klug. Physical principles in the construction of regular viruses. *Cold Spring Harbor Symposia on Quantitative Biology*, 27:1–24, 1962. doi: 10.1101/SQB.1962.027.001.005.

Andy Clark. Whatever next? predictive brains, situated agents, and the future of cognitive science. *Behavioral and Brain Sciences*, 36(3):181–204, 2013. doi: 10.1017/S0140525X12000477.

John H. Conway and Neil J. A. Sloane. Low-dimensional lattices. VII. coordination sequences. *Proceedings of the Royal Society of London. Series A*, 453(1966):2369–2389, 1997. doi: 10.1098/rspa.1997.0126.

John H. Conway and Neil J. A. Sloane. *Sphere Packings, Lattices and Groups*. Springer, New York, 3 edition, 1999. doi: 10.1007/978-1-4757-6568-7.

H. S. M. Coxeter. *Regular Polytopes*. Dover, New York, 3 edition, 1973.

Lancelot Da Costa, Thomas Parr, Noor Sajid, Sebastijan Veselic, Victorita Neacsu, and Karl Friston. Active inference on discrete state-spaces: a synthesis. *Journal of Mathematical Psychology*, 99:102447, 2020. doi: 10.1016/j.jmp.2020.102447.

Lancelot Da Costa, Karl Friston, Conor Heins, and Grigorios A. Pavliotis. Bayesian mechanics for stationary processes. *Proceedings of the Royal Society A*, 477(2256):20210518, 2021. doi: 10.1098/rspa.2021.0518.

A. P. Dempster. Covariance selection. *Biometrics*, 28(1):157–175, 1972. doi: 10.2307/2528966.

Amy C. Edmondson. *A Fuller Explanation: The Synergetic Geometry of R. Buckminster Fuller*. Birkhäuser, Boston, 1987. doi: 10.1007/978-1-4684-7485-5.

P. J. Federico. *Descartes on Polyhedra: A Study of the De Solidorum Elementis*. Sources in the History of Mathematics and Physical Sciences. Springer, New York, 1982. doi: 10.1007/978-1-4612-5759-2.

Miroslav Fiedler. Algebraic connectivity of graphs. *Czechoslovak Mathematical Journal*, 23(2):298–305, 1973. doi: 10.21136/CMJ.1973.101168.

Chris Fields, Karl Friston, James F. Glazebrook, and Michael Levin. A free energy principle for generic quantum systems. *Progress in Biophysics and Molecular Biology*, 173:36–59, 2022. doi: 10.1016/j.pbiomolbio.2022.05.006.

FloatingPragma. Observer patch holography. Git repository, https://github.com/FloatingPragma/observer-patch-holography, 2026. Software, including the Lean development and the model code, is Apache-2.0; papers, documentation, figures, data and ledgers are CC BY-NC-SA 4.0.

Daniel Ari Friedman. QuadMath. Zenodo, 2025. Quadray coordinates, the A3/IVM lattice, omni-numbering and exact tetravolumes. Apache-2.0.

Daniel Ari Friedman. Observer patch holography, the free energy principle, and synergetics: a research dossier. Unpublished working dossier, 2026a.

Daniel Ari Friedman. FEP_Formal. Zenodo, 2026b. Concept DOI, resolving to the latest version; the commit read is pinned in data/sources.json. A standalone catalogue of the Free Energy Principle, Active Inference, Bayesian mechanics, information geometry and thermodynamics, with Lean 4 source. CC BY 4.0.

Daniel Ari Friedman. Observers, blankets, and screens: an integration proposal. Unpublished working proposal, 2026c.

Daniel Ari Friedman. A template/ approach to reproducible generative research: Architecture and ergonomics from configuration through publication. Zenodo, 2026d. The rendering and validation infrastructure this manuscript is built with.

Karl Friston. The free-energy principle: a unified brain theory? *Nature Reviews Neuroscience*, 11(2):127–138, 2010. doi: 10.1038/nrn2787.

Karl Friston. Life as we know it. *Journal of the Royal Society Interface*, 10(86):20130475, 2013. doi: 10.1098/rsif.2013.0475.

Karl Friston. A free energy principle for a particular physics. arXiv:1906.10184, 2019.

Karl Friston and Klaas E. Stephan. Free-energy and the brain. *Synthese*, 159(3):417–458, 2007. doi: 10.1007/s11229-007-9237-y.

Karl Friston, Thomas FitzGerald, Francesco Rigoli, Philipp Schwartenbeck, and Giovanni Pezzulo. Active inference: a process theory. *Neural Computation*, 29(1):1–49, 2017. doi: 10.1162/neco_a_00912.

R. Buckminster Fuller and E. J. Applewhite. *Synergetics: Explorations in the Geometry of Thinking*. Macmillan, New York, 1975.

R. Buckminster Fuller and E. J. Applewhite. *Synergetics 2: Explorations in the Geometry of Thinking*. Macmillan, New York, 1979. URL https://archive.org/details/synergeticsexplo02full.

Carl Friedrich Gauss. Recension der "untersuchungen über die eigenschaften der positiven ternären quadratischen formen" von ludwig august seeber. *Journal für die reine und angewandte Mathematik*, 20:312–320, 1840. doi: 10.1515/crll.1840.20.312. Reprinted from the Göttingische gelehrte Anzeigen of 1831.

Robert Ghrist. *Elementary Applied Topology*. CreateSpace, Seattle, WA, 2014.

Claude Godrèche and Jean-Marc Luck. Characterising the nonequilibrium stationary states of Ornstein–Uhlenbeck processes. *Journal of Physics A: Mathematical and Theoretical*, 52(3):035002, 2019. doi: 10.1088/1751-8121/aaf190.

Michael Goldberg. A class of multi-symmetric polyhedra. *Tohoku Mathematical Journal*, 43:104–108, 1937.

Thomas Hales, Mark Adams, Gertrud Bauer, Tat Dat Dang, John Harrison, Le Truong Hoang, Cezary Kaliszyk, Victor Magron, Sean McLaughlin, Tat Thang Nguyen, Quang Truong Nguyen, Tobias Nipkow, Steven Obua, Joseph Pleso, Jason Rute, Alexey Solovyev, Thi Hoai An Ta, Nam Trung Tran, Thi Diep Trieu, Josef Urban, Ky Vu, and Roland Zumkeller. A formal proof of the Kepler conjecture. *Forum of Mathematics, Pi*, 5:e2, 2017. doi: 10.1017/fmp.2017.1.

Thomas C. Hales. A proof of the Kepler conjecture. *Annals of Mathematics*, 162(3):1065–1185, 2005. doi: 10.4007/annals.2005.162.1065.

Jakob Hansen and Robert Ghrist. Toward a spectral theory of cellular sheaves. *Journal of Applied and Computational Topology*, 3(4):315–358, 2019. doi: 10.1007/s41468-019-00038-7.

Marc Harper. The replicator equation as an inference dynamic. arXiv:0911.1763, 2009.

Josef Hofbauer and Karl Sigmund. *Evolutionary Games and Population Dynamics*. Cambridge University Press, Cambridge, 1998. doi: 10.1017/CBO9781139173179.

John J. Hopfield. Neural networks and physical systems with emergent collective computational abilities. *Proceedings of the National Academy of Sciences*, 79(8):2554–2558, 1982. doi: 10.1073/pnas.79.8.2554.

Adolf Hurwitz. Über die bedingungen, unter welchen eine gleichung nur wurzeln mit negativen reellen theilen besitzt. *Mathematische Annalen*, 46(2):273–284, 1895. doi: 10.1007/BF01446812.

Chii-Ruey Hwang, Shu-Yin Hwang-Ma, and Shuenn-Jyi Sheu. Accelerating gaussian diffusions. *The Annals of Applied Probability*, 3(3):897–913, 1993. doi: 10.1214/aoap/1177005371.

Hassan K. Khalil. *Nonlinear Systems*. Prentice Hall, Upper Saddle River, NJ, 3 edition, 2002.

Gustav Kirchhoff. Über die auflösung der gleichungen, auf welche man bei der untersuchung der linearen vertheilung galvanischer ströme geführt wird. *Annalen der Physik*, 148(12):497–508, 1847. doi: 10.1002/andp.18471481202.

Michael Kirchhoff, Thomas Parr, Ensor Palacios, Karl Friston, and Julian Kiverstein. The markov blankets of life: autonomy, active inference and the free energy principle. *Journal of the Royal Society Interface*, 15(138):20170792, 2018. doi: 10.1098/rsif.2017.0792.

Douglas J. Klein and Milan Randić. Resistance distance. *Journal of Mathematical Chemistry*, 12(1):81–95, 1993. doi: 10.1007/BF01164627.

Solomon Kullback and Richard A. Leibler. On information and sufficiency. *Annals of Mathematical Statistics*, 22(1):79–86, 1951. doi: 10.1214/aoms/1177729694.

Tony Lelièvre, Francis Nier, and Grigorios A. Pavliotis. Optimal non-reversible linear drift for the convergence to equilibrium of a diffusion. *Journal of Statistical Physics*, 152(2):237–274, 2013. doi: 10.1007/s10955-013-0769-x.

Winfried Lohmiller and Jean-Jacques E. Slotine. On contraction analysis for non-linear systems. *Automatica*, 34(6):683–696, 1998. doi: 10.1016/S0005-1098(98)00019-3.

Beren Millidge, Alexander Tschantz, and Christopher L. Buckley. Predictive coding approximates backprop along arbitrary computation graphs. *Neural Computation*, 34(6):1329–1368, 2022. doi: 10.1162/neco_a_01497.

Bernhard Mueller. Agreement and surprise: Local repair, dynamics and the limits of equilibrium. Preprint, Pragma Research Inc., 22 October 2026. PhilPapers record MUEAAS-2, 2026. URL https://philpapers.org/rec/MUEAAS-2.

Bernhard Mueller, Mario Poneder, Alexander Osika, Kai Xue, Ben Cassie, Peter Nguyen, Jinwook Kim, David Matscheko, Daniel Ari Friedman, Jonathan Hill, William T. Glynn, Maarten Antonie Visser, Kale Arnav Anirudha, and Brieuc de La Fournière. Observers who read their universe into existence: Finite consensus and the reconstruction of standard physics. Preprint. PhilPapers record MUEFOC, 2026. URL https://philpapers.org/rec/MUEFOC.

Thomas Parr, Lancelot Da Costa, and Karl Friston. Markov blankets, information geometry and stochastic thermodynamics. *Philosophical Transactions of the Royal Society A*, 378(2164):20190159, 2020. doi: 10.1098/rsta.2019.0159.

Thomas Parr, Giovanni Pezzulo, and Karl J. Friston. *Active Inference: The Free Energy Principle in Mind, Brain, and Behavior*. MIT Press, Cambridge, MA, 2022. doi: 10.7551/mitpress/12441.001.0001.

Judea Pearl. *Probabilistic Reasoning in Intelligent Systems: Networks of Plausible Inference*. Morgan Kaufmann, San Mateo, CA, 1988. URL https://www.sciencedirect.com/book/monograph/9780080514895.

Fernando J. Pineda. Generalization of back-propagation to recurrent neural networks. *Physical Review Letters*, 59(19): 2229–2232, 1987. doi: 10.1103/PhysRevLett.59.2229.

Michael Robinson. *Topological Signal Processing*. Springer, Berlin, 2014. doi: 10.1007/978-3-642-36104-3.

Edward John Routh. *A Treatise on the Stability of a Given State of Motion*. Macmillan, London, 1877.

Håvard Rue and Leonhard Held. *Gaussian Markov Random Fields: Theory and Applications*. Chapman and Hall/CRC, Boca Raton, FL, 2005. doi: 10.1201/9780203492024.

Noor Sajid, Philip J. Ball, Thomas Parr, and Karl J. Friston. Active inference: demystified and compared. *Neural Computation*, 33(3):674–712, 2021. doi: 10.1162/neco_a_01357.

Benjamin Scellier and Yoshua Bengio. Equilibrium propagation: bridging the gap between energy-based models and backpropagation. *Frontiers in Computational Neuroscience*, 11:24, 2017. doi: 10.3389/fncom.2017.00024.

Kurt Schütte and Bartel Leendert van der Waerden. Das problem der dreizehn kugeln. *Mathematische Annalen*, 125(1): 325–334, 1953. doi: 10.1007/BF01343127.

Udo Seifert. Stochastic thermodynamics, fluctuation theorems and molecular machines. *Reports on Progress in Physics*, 75 (12):126001, 2012. doi: 10.1088/0034-4885/75/12/126001.

Siavash Shahshahani. A new mathematical framework for the study of linkage and selection. *Memoirs of the American Mathematical Society*, 17(211), 1979. doi: 10.1090/memo/0211.

Claude E. Shannon. A mathematical theory of communication. *Bell System Technical Journal*, 27(3):379–423, 1948. doi: 10.1002/j.1538-7305.1948.tb01338.x. Part I; continued in volume 27, number 4, pages 623–656.

Peter D. Taylor and Leo B. Jonker. Evolutionary stable strategies and game dynamics. *Mathematical Biosciences*, 40(1–2): 145–156, 1978. doi: 10.1016/0025-5564(78)90077-9.

H. F. Verheyen. The complete set of Jitterbug transformers and the analysis of their motion. *Computers & Mathematics with Applications*, 17(1–3):203–250, 1989. doi: 10.1016/0898-1221(89)90160-0.

James C. R. Whittington and Rafal Bogacz. An approximation of the error backpropagation algorithm in a predictive coding network with local Hebbian synaptic plasticity. *Neural Computation*, 29(5):1229–1262, 2017. doi: 10.1162/NECO_a_00949.